







Induction of T-helper-17-cell-mediated anti-tumour immunity by pathogen-mimicking polymer nanoparticles

Received: 17 May 2021

Accepted: 26 October 2022

Published online: 23 December 2022

 Check for updates

Sejin Son ^{1,2,3,4,5,12} ✉, Jutaek Nam ^{1,2,6,12}, April S. Kim^{1,2}, Jinsung Ahn^{2,7},
Kyung Soo Park ^{2,8}, May Thazin Phoo^{2,8}, Brett Sherren³, Weiping Zou ⁹,
Soo-Hong Lee⁷, Omid C. Farokhzad ^{3,10}, Jinjun Shi³ & James J. Moon ^{1,2,8,11} ✉

The effectivity of cancer immunotherapies is hindered by immunosuppressive tumour microenvironments that are poorly infiltrated by effector T cells and natural killer cells. In infection and autoimmune disease, the recruitment and activation of effector immune cells is coordinated by pro-inflammatory T helper 17 (T_H17) cells. Here we show that pathogen-mimicking hollow nanoparticles displaying mannan (a polysaccharide that activates T_H17 cells in microbial cell walls) limit the fraction of regulatory T cells and induce T_H17-cell-mediated anti-tumour responses. The nanoparticles activate the pattern-recognition receptor Dectin-2 and Toll-like receptor 4 in dendritic cells, and promote the differentiation of CD4⁺ T cells into the T_H17 phenotype. In mice, intra-tumoural administration of the nanoparticles decreased the fraction of regulatory T cells in the tumour while markedly increasing the fractions of T_H17 cells (and the levels of T_H17-cell-associated cytokines), CD8⁺ T cells, natural killer cells and M1-like macrophages. The anti-tumoural activity of the effector cells was amplified by an agonistic antibody against the co-stimulatory receptor OX40 in multiple mouse models. Nanomaterials that induce T_H17-cell-mediated immune responses may have therapeutic potential.

Microbial pathogens present ‘danger’ signals at the site of infection, and confer protective immunity by inducing pro-inflammatory cytokines and mobilizing leucocytes^{1–3}. During microbial infection, pathogen-associated molecular patterns (PAMPs) activate pattern-recognition receptors (PRRs) expressed on innate immune

cells, such as dendritic cells³ (DCs), leading to the production of pro-inflammatory cytokines, including IL-1 β , IL-6 and IL-23, that promote the differentiation and stabilization of T helper 17 (T_H17) cells^{4,5}. T_H17 cells are a subset of CD4⁺ helper T cells defined by IL-17A expression, and play crucial roles in the host’s defence against infectious

¹Department of Pharmaceutical Sciences, University of Michigan, Ann Arbor, MI, USA. ²Biointerfaces Institute, University of Michigan, Ann Arbor, MI, USA. ³Center for Nanomedicine and Department of Anesthesiology, Brigham and Women’s Hospital, Harvard Medical School, Boston, MA, USA.

⁴Department of Biological Sciences, Inha University, Incheon, Republic of Korea. ⁵Department of Biological Sciences and Bioengineering, Inha University/ Industry-Academia Interactive R&E Center for Bioprocess Innovation, Inha University, Incheon, Republic of Korea. ⁶College of Pharmacy, Chonnam National University, Gwangju, Republic of Korea. ⁷Department of Biomedical Engineering, Dongguk University, Seoul, Republic of Korea. ⁸Department of Biomedical Engineering, University of Michigan, Ann Arbor, MI, USA. ⁹Department of Surgery, University of Michigan, Ann Arbor, MI, USA. ¹⁰Seer, Inc., Redwood City, CA, USA. ¹¹Department of Chemical Engineering, University of Michigan, Ann Arbor, MI, USA. ¹²These authors contributed equally:

Sejin Son, Jutaek Nam. ✉ e-mail: ssejin@inha.ac.kr; moon@med.umich.edu

agents, including fungi, bacteria and viruses, by recruiting and activating effector T lymphocytes at the site of microbial infection⁶. In addition to their roles in infection, T_H17 cells are major drivers of autoimmune diseases, which has prompted intensive research into the development of therapeutics for suppressing T_H17 cells in autoimmune diseases, with several clinical trials underway^{7–13}. In stark contrast, the role of T_H17 cells in cancer progression and therapy remains under debate^{14,15}. There are reports of adoptively transferred T_H17 cells causing tumour regression in mice, and tumour-associated IL-17 correlating with survival of patients with cancer^{16–19}. However, apart from a few studies reporting T_H17-inducing immunosuppressant agents or peptide-based fibres for vaccination against infectious pathogens^{8,20,21}, it remains largely unknown how to induce T_H17 cells in vivo, without expanding their immunosuppressive counterpart (regulatory T cells; T_{reg} cells) for successful cancer immunotherapy. In this Article, we report a synthetic 'nano-PAMP' that tips the balance between T_H17 cells and T_{reg} cells towards pro-inflammatory T_H17 cells, with potent anti-tumour efficacy.

Importantly, fungal infection caused by the yeast *Candida albicans* has been shown to trigger Dectin-2 and Toll-like receptor (TLR)-4 activation in DCs and to generate T_H17 immunity^{22,23}. Dectin-2 signalling promotes IL-6, IL-1 β and IL-23, which drive T_H17 cell differentiation and maintenance^{22,23}, and TLR-4-dependent maturation of DCs has been reported to contribute to T_H17 immunity²⁴. Notably, ~90% of the outer cell wall of *Candida albicans* is composed of polysaccharides, including mannan, glucan and chitin^{3,25} among these, mannan, composed of an α -(1,6) mannose backbone with α -(1,2)- or α -(1,3)-linked oligomannose side chains, is a ligand for Dectin-2 (refs. 23,26). Therefore, we hypothesized that the multivalent display of mannan on a pathogen-mimicking system may serve as a potent stimulator of T_H17 response.

We have recently reported the development of *Saccharomyces cerevisiae* mannan-based nanocapsules (Mann-NC) for subcutaneous delivery of messenger-RNA-based vaccines²⁷. *S. cerevisiae* is a yeast widely used in winemaking, baking and brewing, and its mannan has close structural similarity to that from *C. albicans*. Here we show that Mann-NC composed of mannan (without any other cargo) is a potent nano-PAMP for Dectin-2 and TLR-4 activation and that the intra-tumoural administration of Mann-NC generates robust T_H17 responses (Fig. 1a,b). PAMP–PRR interaction is controlled by the geometry, nanoscale arrangement and architecture of PAMP on microbes that dictate the accessibility and availability of PRR engagement^{28,29}. Mann-NC has several favourable features as a nano-PAMP, including its bioactive ingredients without any pathogenic substance; tunable nanoscopic dimension and shape; and multivalent surface PAMP arrangement with structural flexibility for favourable PRR engagement. Intra-tumoural administration of Mann-NC induces the release of cytokines and chemokines, including CXCL10 and CCL2, resulting in the recruitment and activation of anti-tumour CD8⁺ T cells, natural killer (NK) cells and M1-like macrophages within the tumour microenvironment (TME) (Fig. 1a). Moreover, the anti-tumour efficacy of Mann-NC was further amplified when combined with an agonistic antibody against OX40 (α OX40), which is a co-stimulatory receptor expressed on activated effector cells, including CD4⁺ T cells, CD8⁺ T cells and NK cells, and has been shown to augment the functions of T_H17 cells^{30,31}. Overall, we present a strategy for redirecting anti-pathogen immune responses to cancer immunotherapy using a pathogen-mimicking synthetic nano-PAMP.

Results and discussion

Preparation and characterization of Mann-NC

Mann-NC was prepared by employing silica nanoparticles (siNPs) as a sacrificial template²⁷. Briefly, siNPs were coated with polyethyleneimine (PEI), reacted with oxidized mannan to form imine-mediated conjugates, and then removed by chemical dissolution to obtain hollow Mann-NCs (Fig. 1b and Extended Data Fig. 1). After the core templates were removed, Mann-NC was composed of mostly mannan

(~93% mannan and ~7% PEI by weight), compactly packed in a thin nanoscale capsule surface for multivalent presentation and potent immune modulation. Transmission electron microscopy (TEM) images show core-empty capsule structure of Mann-NC with a size comparable to an siNP template (Fig. 1c). The hydrodynamic size and zeta potential were measured as 200 ± 3.3 nm and -46 ± 1.4 mV, and 230 ± 10.3 nm and 5 ± 0.02 mV for siNP and Mann-NC, respectively (Supplementary Fig. 1). Atomic force microscopy (AFM) analyses corroborated the deformable spherical morphology of Mann-NCs in wet or dried condition (Fig. 1d) and revealed that the well thickness of Mann-NC is approximately 10 nm in dried condition (Fig. 1e).

Mann-NC triggers robust immune activation in vitro

Mann-NC is expected to promote engagement of mannan to its target PRRs via multivalent interactions by displaying mannan on the surface with high density and structural flexibility (Fig. 2a). To test this idea, we compared Mann-NC and its native, soluble mannan counterpart (Native-Mann) for the activation of bone marrow-derived dendritic cells (BMDCs). Cy5.5-tagged Mann-NC was gradually taken up by BMDCs over 2 h of incubation, whereas only a marginal uptake was observed for Cy5.5-tagged Native-Mann (Fig. 2b). Mann-NC and Native-Mann both induced slight proliferation of BMDCs without any notable cytotoxicity (Fig. 2b). Confocal images revealed that Mann-NCs were efficiently internalized by BMDCs after 4 h, whereas Native-Mann was barely detected in the cells (Fig. 2c). BMDCs incubated with Mann-NC exhibited many outgrowing dendrites, suggesting maturation and activation. Indeed, Mann-NC induced stronger DC activation than Native-Mann, as shown by the significantly increased surface expression of CD40, CD86 and MHC-II activation markers and increased secretion of IL-12p70, TNF- α and IL-6 pro-inflammatory cytokines (Fig. 2d,e). These results showed that multivalent surface presentation of mannan on Mann-NC enhanced engagement, cellular uptake and activation of BMDCs, compared with Native-Mann.

Mann-NC engages Dectin-2 and TLR-4 on DCs

Next, we sought to identify specific PRRs that interact with Mann-NC. Notably, mannan is known to interact with Dectin-2, Mincle, TLR-2 and TLR-4 (refs. 32,33). BMDCs were pre-treated for 30 min with blocking antibodies against Dectin-1, Dectin-2, CD206, CD209, Mincle, TLR-2 or TLR-4, and then incubated for 12 h with either Mann-NC or Native-Mann, followed by TNF- α measurement in medium as a marker for immune activation. BMDCs pre-treated with antibodies against Dectin-2 or TLR-4 produced significantly decreased amount of TNF- α after Mann-NC treatment ($P < 0.0001$; Fig. 2f), suggesting that Dectin-2 and TLR-4 are the major PRRs for Mann-NC. We observed a similar trend, but to a lesser degree, for Native-Mann (Fig. 2f). Corroborating these results, both Native-Mann and Mann-NC activated human embryonic kidney (HEK) reporter cells expressing Dectin-2 or TLR-4, but not Dectin-1 or TLR-2 reporter cell lines (Fig. 2g). Interestingly, compared with Native-Mann, Mann-NC induced significantly stronger activation of Dectin-2 and TLR-4 ($P < 0.0001$; Fig. 2g), indicating that multivalent presentation of mannan on nanocapsules significantly improved PRR activation. However, addition of antibodies against Dectin-2 or TLR-4 did not inhibit cellular uptake of Mann-NC by BMDCs (Supplementary Fig. 2). Instead, cellular uptake of Mann-NC was significantly decreased in the presence of dextran sulfate³⁴ or chlorpromazine³⁵, which are inhibitors of scavenger receptor class A-mediated endocytosis and clathrin-mediated endocytosis, respectively (Fig. 2h,i). In contrast, pharmacological inhibitors of micropinocytosis/phagocytosis (cytochalasinD)³⁵ or lipid rafts/cholesterol-enriched microdomains/caveolae (methyl- β -cyclodextrin, M β -CD)³⁵ did not impact the cellular uptake of Mann-NC (Fig. 2h,i). Taken together, Mann-NC are taken up by DCs via scavenger receptor class A- and clathrin-dependent endocytosis, leading to Dectin-2- and TLR-4-mediated immune activation.

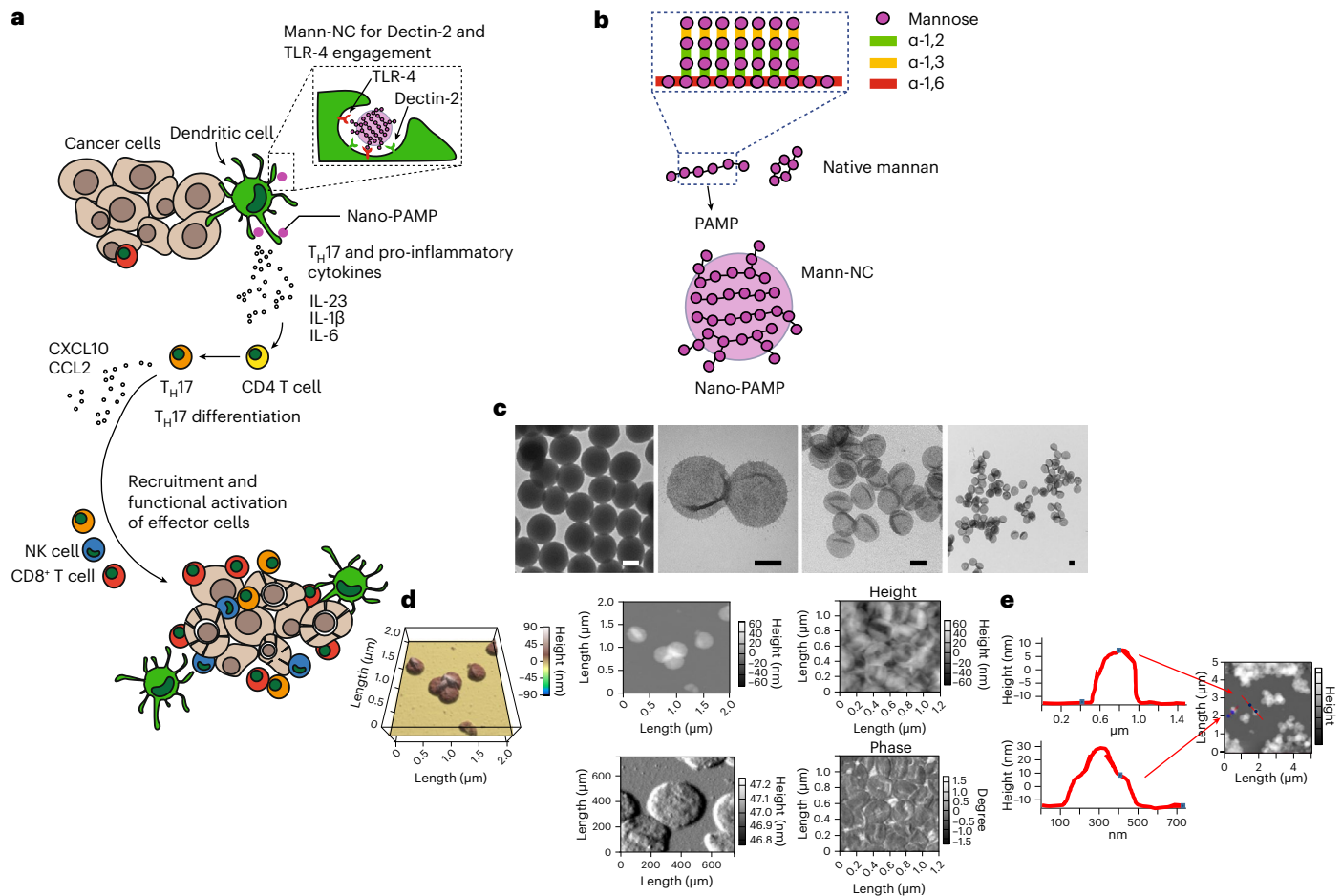


Fig. 1 | Mann-NC for cancer immunotherapy. **a**, Mann-NC is a nano-PAMP that engages Dectin-2 and TLR-4 on DCs for T_H17 -skewed immune activation. T_H17 cells supported by IL-23, IL-6 and IL-1 β orchestrate the intra-tumoural recruitment of $CD8^+$ T cells and NK cells via chemokines, including CXCL10 and CCL2, leading to potent anti-tumour efficacy. **b**, Mann-NC is composed of mannan with α -(1,6) mannoside backbone and α -(1,2) and α -(1,3) mannoside side chains. **c**, TEM images of a template siNP and hollow Mann-NCs. Scale bars, 100 nm. **d, e**, AFM images show Mann-NC in dried (top) and wet conditions (bottom) (**d**) and wall thickness of Mann-NC measured in dried condition (**e**).

mannoside backbone and α -(1,2) and α -(1,3) mannoside side chains. **c**, TEM images of a template siNP and hollow Mann-NCs. Scale bars, 100 nm. **d, e**, AFM images show Mann-NC in dried (top) and wet conditions (bottom) (**d**) and wall thickness of Mann-NC measured in dried condition (**e**).

Mann-NC drives T_H17 differentiation of $CD4^+$ T cells

Next, given Mann-NC-mediated activation Dectin-2 and TLR-4, and previous reports of Dectin-2- and TLR-4-mediated DC activation of T_H17 cells^{22,23}, we examined whether Mann-NC can promote DCs to induce T_H17 differentiation of $CD4^+$ T cells. To examine this, BMDCs were incubated with Mann-NC for 12 h, and the conditioned medium was added to naïve $CD4^+$ T cells. After 5 days of culture, $CD4^+$ T cells were examined for their functional phenotype by intracellular cytokine staining (ICS) after restimulation with phorbol 12-myristate 13-acetate (PMA) and ionomycin. While Native-Mann induced IL-17 $^+$ $CD4^+$ T cells in a dose-dependent manner (Fig. 2j), Mann-NC significantly increased the induction of IL-17 $^+$ $CD4^+$ T cells across all doses tested ($P < 0.0001$, Fig. 2j,k). On the other hand, Mann-NC had a minimal impact on IL-4 $^+$, IFN- γ $^+$ or Foxp3 $^+$ $CD4^+$ T cells (Fig. 2k and Supplementary Fig. 3). We have also confirmed that Mann-NC treatment during DC-mediated priming of p31 antigen-specific BDC2.5 $CD4^+$ T cells skewed their differentiation towards IL-17 $^+$ $CD4^+$ T-cell phenotype (Extended Data Fig. 2a). These results suggest that during $CD4^+$ T-cell priming by DCs, DCs stimulated by Mann-NC trigger the differentiation of $CD4^+$ T cells towards T_H17 phenotype. Next, we examined whether the interactions between Mann-NC and Dectin-2 and/or TLR-4 on DCs play any role in T_H17 differentiation. BMDCs were pre-incubated with blocking antibodies against Dectin-2 or TLR-4, followed by incubation with Mann-NC. Mann-NC-conditioned media were then added to naïve $CD4^+$ T cells. The frequency of IL-17 $^+$

$CD4^+$ T cells was significantly reduced when T cells were supplemented with Mann-NC-conditioned media pre-treated with blocking antibodies against Dectin-2 or TLR-4 ($P < 0.0001$; Fig. 2l). In contrast, the presence of blocking antibodies against Dectin-1 or TLR-2 had a minimal impact. Taken together, these results show that Mann-NC activates Dectin-2 and TLR-4 on DCs, resulting in strong induction of T_H17 -phenotype $CD4^+$ T cells.

Mann-NC activates innate immune cells and T_H17 cells

T_H17 cells are known to orchestrate the recruitment and activation of NK and $CD8^+$ T cells by producing various cytokines and chemokines (for example, CCL2 (refs. 16,36) and CXCL10 (ref. 17)), thus leading to anti-tumour effects³⁷. Motivated by the T_H17 -inducing property of Mann-NC observed in vitro, we examined the therapeutic potential of Mann-NC in murine tumour models. BALB/c mice were inoculated subcutaneously with CT26 colon carcinoma cells on day 0, followed by intra-tumoural administration of PBS, Native-Mann or Mann-NC on days 9, 12 and 15 (Fig. 3a). Mann-NC therapy significantly slowed the tumour growth and extended the animal survival (Fig. 3b,c). Interestingly, intra-tumoural administration of Native-Mann also exhibited modest anti-tumour effects (Fig. 3b,c). We examined the immune landscape of the TME on day 15 and observed that Mann-NC therapy markedly increased the frequency of $CD45^+$ leucocytes, compared with PBS and Native-Mann (Fig. 3d). Mann-NC significantly elevated the

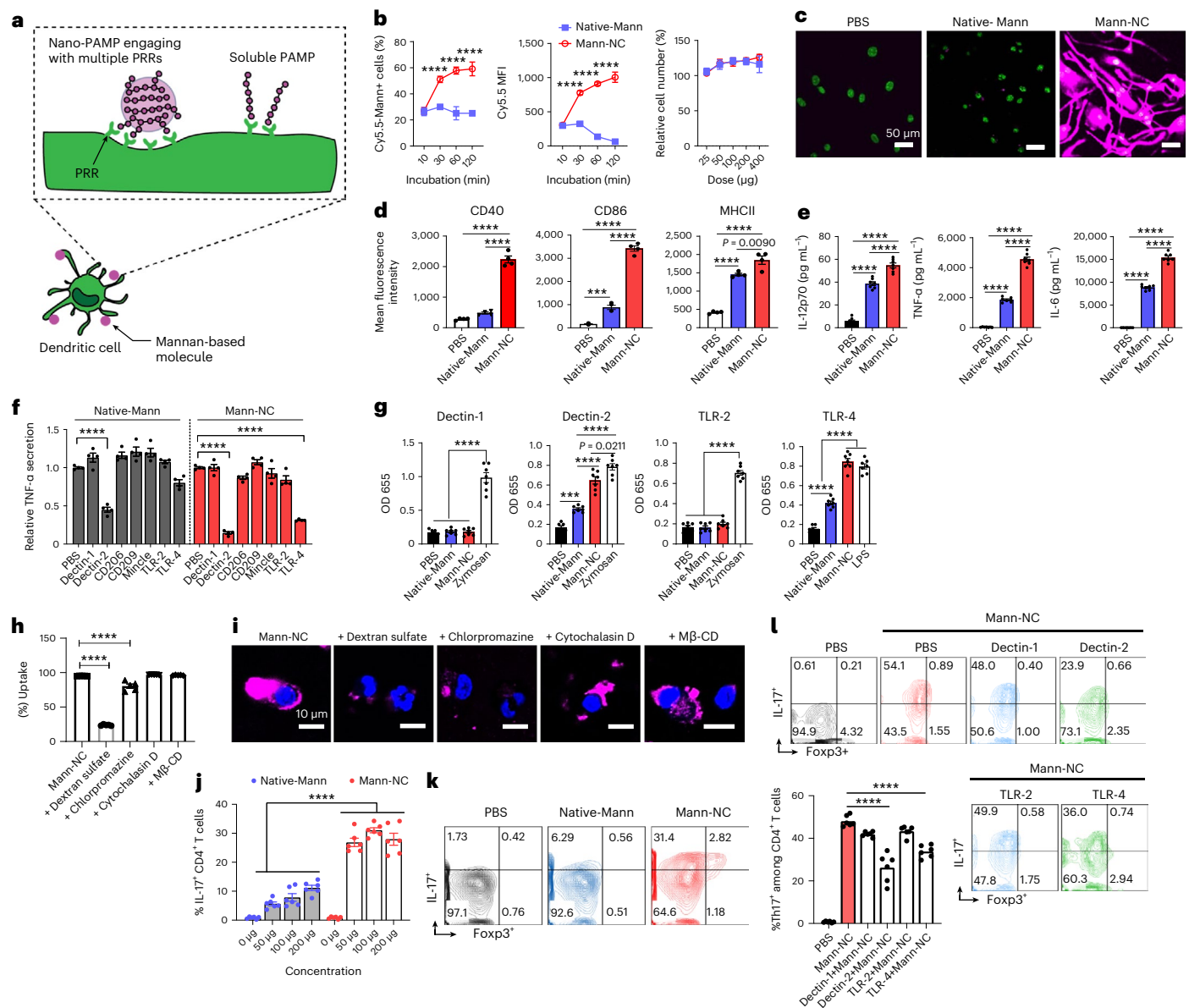


Fig. 2 | Mann-NC activates Dectin-2 and TLR-4 and induces IL-17⁺ CD4⁺ T cells. **a**, Schematic illustration of Mann-NC interacting with multiple PRRs for enhanced immune activation. **b–e**, BMDCs were incubated with Mann-NC or Native-Mann and examined for cellular uptake of Cy5.5-tagged mannan and cell number relative to the PBS control (**b**), confocal microscope images taken after 4 h of sample incubation (**c**), upregulation of activation markers on DCs (that is, CD40, CD86 and MHC-II) measured by flow cytometry (**d**), and secretion of pro-inflammatory cytokines (that is, IL12p70, TNF- α and IL-6) by ELISA (**e**). **f**, BMDCs were pre-treated with blocking antibodies against PRRs for 30 min and then incubated with Mann-NC or Native-Mann, followed by measurement of TNF- α release. **g**, HEK reporter cell lines were used to examine Dectin-1, Dectin-2, TLR-2 or TLR-4 engagement with Mann-NC. **h, i**, Cellular uptake of Mann-NC by BMDCs was assessed after 1 h of co-incubation of various pharmacological inhibitors,

followed by examination by flow cytometry (**h**) and confocal microscopy (**i**). **j, k**, Conditioned media from BMDCs pulsed with Native-Mann or Mann-NC for 12 h were added to naive CD4⁺ T cells. After 5 days of culture, ICS was performed by incubating CD4⁺ T cells with PMA, ionomycin and Brefeldin A for 4 h. Shown are the quantification of IL-17⁺ CD4⁺ T cells (**j**) and their representative contour plots for IL-17⁺ CD4⁺ and Foxp3⁺ CD4⁺ T cells (**k**). **l**, The frequencies of IL-17⁺ CD4⁺ T cells were measured after adding blocking antibodies against Dectin-1, Dectin-2, TLR-2 or TLR-4 during co-culture of BMDCs with Mann-NC, followed by naive CD4⁺ T-cell culture as in **j**, and the representative contour plots are shown. Data represent mean \pm standard error of the mean (s.e.m.), from a representative experiment ($n = 4$ (**b, d–f**) or $n = 6$ (**g–l**)) from two (**c, h–k**) or three (**b, d–g, l**) independent experiments. **** $P < 0.001$, **** $P < 0.0001$, analysed by one-way (**d–h, l**) or two-way (**b, j**) ANOVA with Bonferroni’s multiple comparisons test.

intra-tumoural frequency of CD11c⁺ DCs and their maturation as shown by CD80 surface staining (Fig. 3e). In addition, Mann-NC significantly increased the frequency of CD8 α ⁺ CD103⁺ CD11c⁺ DCs ($P < 0.0001$; Fig. 3e), which is a critical DC subset for the induction of CD8⁺ cytotoxic T lymphocytes^{38,39}. Mann-NC also increased the frequency of activated monocytes (Fig. 3f) and markedly increased the frequency of pro-inflammatory M1-like CD80⁺ F4/80⁺ macrophages without changing the frequency of M2-like macrophages (Fig. 3g). This resulted in a

significantly increased M1/M2 ratio for the Mann-NC group, compared with Native-Mann (Fig. 3g). On the other hand, Mann-NC treatment did not significantly change the frequency of myeloid-derived suppressor cells (MDSCs) (Supplementary Fig. 4). Next, we investigated how Mann-NC affects CD4⁺ T-cell differentiation in vivo by analysing TME and tumour-draining lymph nodes (tdLNs). While Mann-NC treatment did not affect the frequency of CD4⁺ T cells in the tumours (Supplementary Fig. 5a), Mann-NC induced upregulation of OX40 on CD4⁺

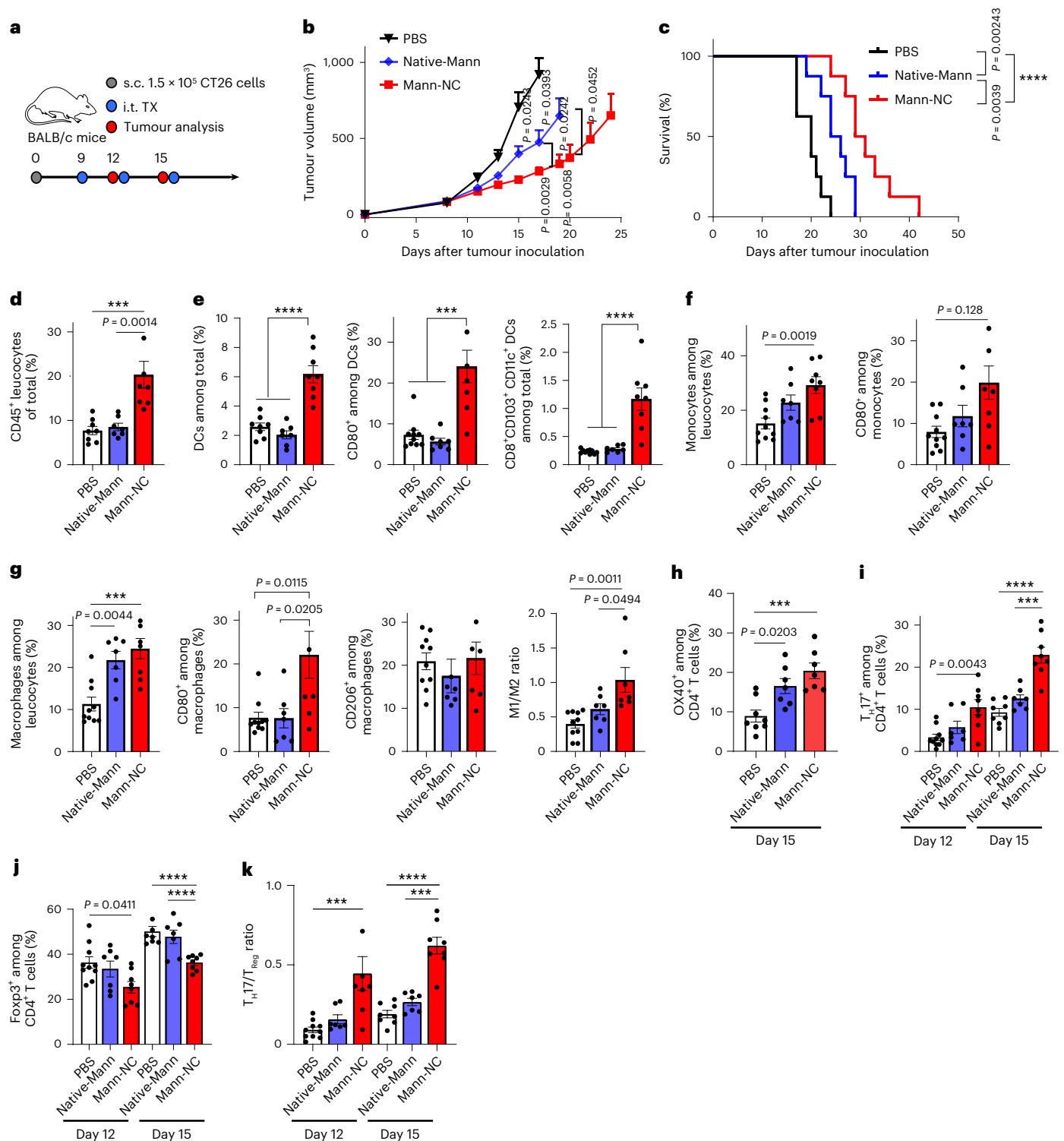


Fig. 3 | Mann-NC activates innate immune cells and T_H17 cells and exerts anti-tumour effect. **a**, BALB/c mice were inoculated subcutaneously (s.c.) with 1.5×10^5 CT26 cells on day 0 and treated by intra-tumoural treatment (i.t. TX) with Mann-NC on days 9, 12 and 15. **b,c**, Average tumour growth (b) and survival curves (c). **d–g**, Tumour tissues were analysed on day 15 for CD45⁺ leucocytes (d), CD11c⁺, CD80⁺ CD11c⁺, and CD8⁺ CD103⁺ CD11c⁺ DCs (e), Ly6C⁺ and Ly6C⁺ CD80⁺ monocytes (f), and F4/80⁺, F4/80⁺ CD80⁺ M1-like and F4/80⁺ CD206⁺ M2-like macrophages, and the corresponding M1/M2 ratio (g). **h–k**, Tumour tissues were

analysed for the frequencies of OX40⁺ CD4⁺ T cells on day 15 (h); the frequencies of IL-17⁺ CD4⁺ T_H17 cells (i), Foxp3⁺ CD4⁺ T_{reg} cells (j) and the corresponding T_H17/T_{reg} ratio within the TME (k). Data represent mean \pm s.e.m., from a representative experiment ($n = 7$ for Mann-NC or 8 for PBS and Native-Mann (b,c) and $n = 7$ for Native-Mann or 8 for PBS and Mann-NC (d–k) biologically independent samples) from two (h) or three (b–g,i–k) independent experiments. *** $P < 0.001$, **** $P < 0.0001$, analysed by one-way (d–h) or two-way (b,h–k) ANOVA with Bonferroni’s multiple comparisons test, or log-rank (Mantel–Cox) test (c).

T cells and T_{reg} cells (Fig. 3h and Extended Data Fig. 2b), but not PD-1 on CD4⁺ T cells (Supplementary Fig. 5b). Importantly, Mann-NC markedly increased the frequency of IL-17⁺ CD4⁺ T cells on days 12 ($P < 0.01$) and

15 ($P < 0.0001$) (Fig. 3i and Supplementary Fig. 6), with a concomitant decrease in the frequency of Foxp3⁺ CD4⁺ T_{reg} cells (Fig. 3j and Supplementary Fig. 6). This resulted in a significantly elevated T_H17/T_{reg}

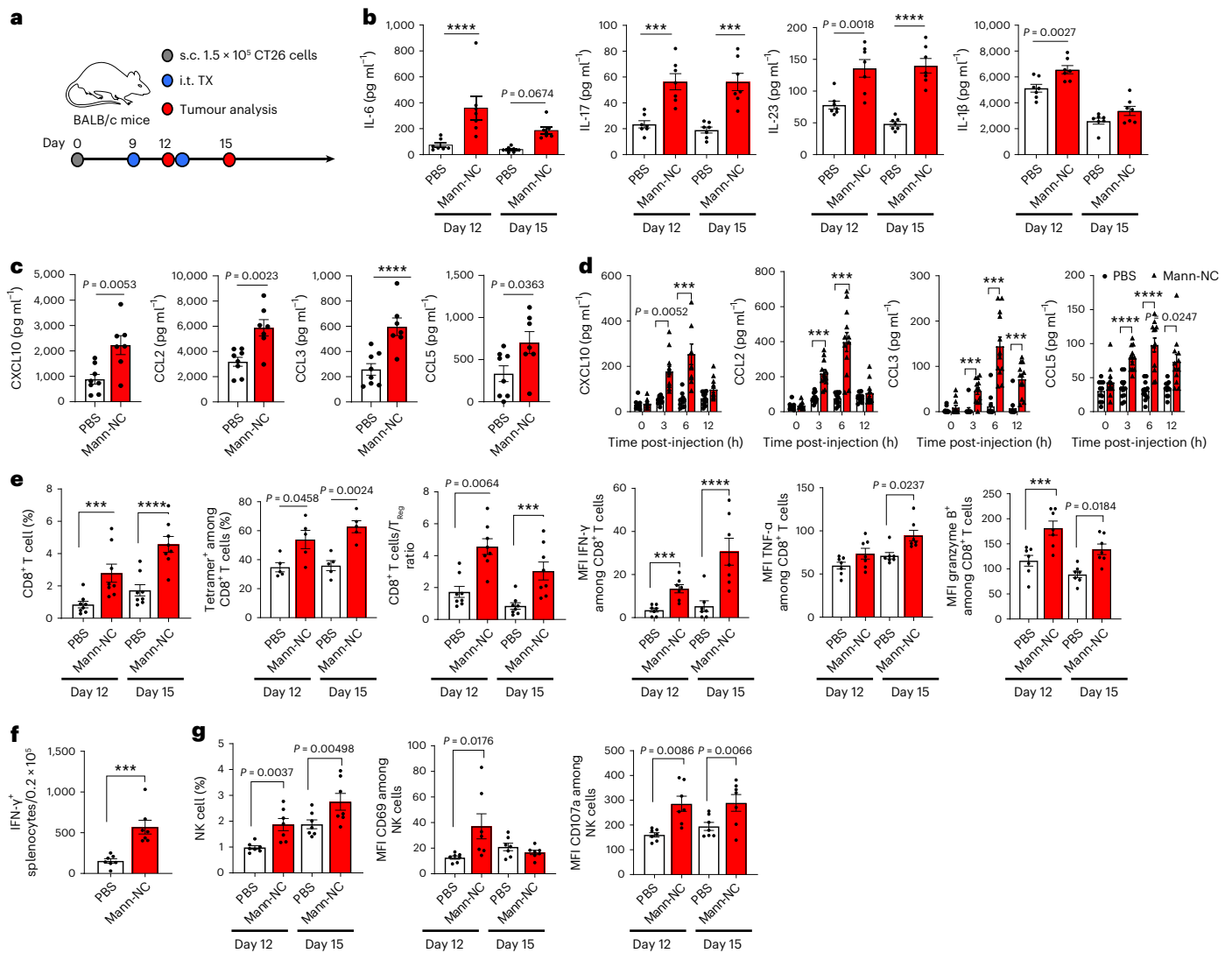


Fig. 4 | Mann-NC induces T_H17 -associated cytokines and chemokines and promotes $CD8^+$ T-cell and NK cell responses. **a**, BALB/c mice were inoculated subcutaneously (s.c.) with 1.5×10^5 CT26 cells on day 0 and treated by intratumoural (i.t.) administration of Mann-NC on days 9 and 12. Tumour tissues were analysed after 3 days of each treatment. **b**, Intra-tumoural concentrations of IL-6, IL-17, IL-23 and IL-1 β . **c, d**, Intra-tumoural (**c**) and serum (**d**) concentrations of CXCL10, CCL2, CCL3 and CCL5 measured on day 15 (**c**) and on day 9 (**d**). **e**, Intra-tumoural frequencies of $CD8^+$ T cells, AH-1 tetramer $^+$ $CD8^+$ T cells, the ratio of

$CD8^+$ T cells to T_{reg} cells, and the expression levels of IFN- γ , TNF- α and granzyme B. **f**, IFN- γ ELISPOT analysis performed on day 15 after restimulation of splenocytes with AH-1 peptide. **g**, Intra-tumoural frequencies of NK cells and their expression levels of CD69 and CD107a. Data represent mean \pm s.e.m., from a representative experiment ($n = 7$ (**b, c, e–g**) and $n = 12$ (**d**)) biologically independent samples) from two (**b–d, f**) or three (**e, g**) independent experiments. *** $P < 0.001$, **** $P < 0.0001$, analysed by two-way ANOVA with Bonferroni’s multiple comparisons test (**b, d, e, g**) or unpaired two-tailed Student’s *t*-test (**c, f**).

ratio within the TME for the Mann-NC-treated mice (Fig. 3k). We also observed a similar trend in the frequencies of $CD4^+$ T cells, $T_H17^+ CD4^+$ T cells and $Foxp3^+ CD4^+$ T_{reg} cells and T_H17/T_{reg} ratio in tdLNs (Extended Data Fig. 2c–f). In contrast, Mann-NC did not change the frequencies of T_H1 cells or T_H2 cells (Extended Data Fig. 2g). Taken together, Mann-NC is a potent innate immune stimulator that shifts the T_H17/T_{reg} balance towards T_H17 immunity in tumour-bearing mice.

Mann-NC activates intra-tumoural $CD8^+$ T cells and NK cells

On the basis of the strong T_H17 -inducing capacity of Mann-NC, we next focused on the Mann-NC formulation and studied the impact of T_H17 immune response primed by Mann-NC on the cytokine and chemokine profiles and other effector immune cells (Fig. 4a). Intra-tumoural administration of Mann-NC led to significantly elevated levels of T_H17 -associated cytokines, including IL-6, IL-17, IL-23 and IL-1 β (refs. 4,5,40) as well as pro-inflammatory chemokines, including CXCL10, CCL2, CCL3 and CCL5, within the TME (Fig. 4b,c). We also observed

their increased concentrations in serum, which peaked after 6 h of Mann-NC administration (Fig. 4d). Flow cytometric analysis of tumour tissues indicated that Mann-NC was taken up mostly by intra-tumoural DCs, monocytes, macrophages and neutrophils, but not by tumour cells (Extended Data Fig. 3). Dectin-2 and TLR-4 were expressed among intra-tumoural DCs, macrophages, monocytes and neutrophils, and Mann-NC treatment did not change their expression levels (Supplementary Fig. 7). In particular, CXCL10, CCL2, CCL3 and CCL5 are important chemokines associated with tumour infiltration of effector immune cells⁴¹. Thus, we next examined the impact of Mann-NC treatment on the intra-tumoural frequencies of key effector cells, that is, $CD8^+$ T cells and NK cells. Indeed, Mann-NC treatment significantly increased the frequency of total $CD8^+$ T cells, $CD8^+$ T cells against tumour-specific AH-1 antigen (H-2L^d-restricted gp70_{423–431}, an immunodominant $CD8^+$ T-cell epitope in CT26 tumour cells), the ratio of intra-tumoural $CD8^+$ T cells to T_{reg} cells, as well as IFN- γ ⁺, TNF- α ⁺ and granzyme B⁺ $CD8^+$ T cells (Fig. 4e). Mice treated with Mann-NC also exhibited a 3.7-fold higher

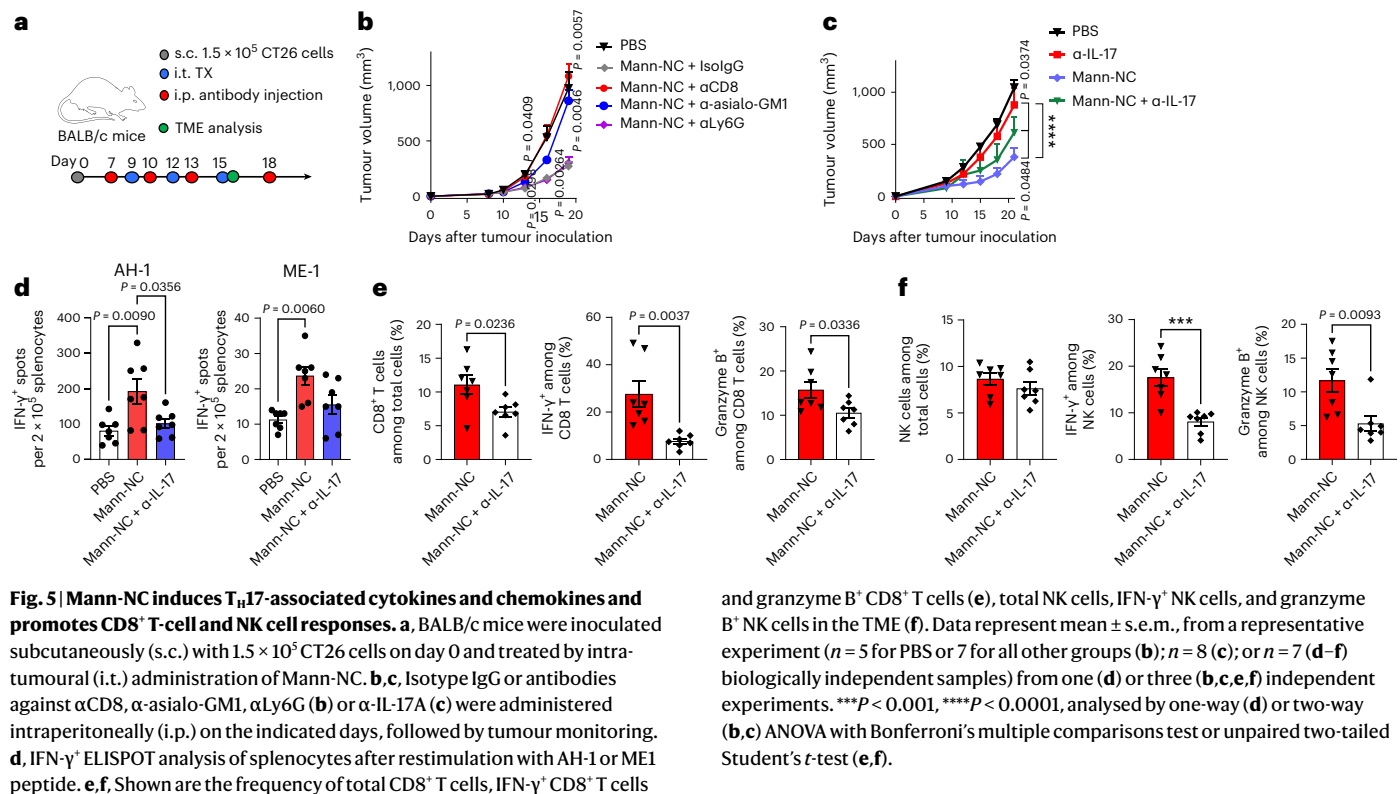


Fig. 5 | Mann-NC induces T_H17-associated cytokines and chemokines and promotes CD8⁺ T-cell and NK cell responses. **a**, BALB/c mice were inoculated subcutaneously (s.c.) with 1.5×10^5 CT26 cells on day 0 and treated by intra-tumoural (i.t.) administration of Mann-NC. **b,c**, Isotype IgG or antibodies against α CD8, α -asialo-GM1, α Ly6G (**b**) or α -IL-17A (**c**) were administered intraperitoneally (i.p.) on the indicated days, followed by tumour monitoring. **d**, IFN- γ ELISPOT analysis of splenocytes after restimulation with AH-1 or ME1 peptide. **e,f**, Shown are the frequency of total CD8⁺ T cells, IFN- γ CD8⁺ T cells

and granzyme B⁺ CD8⁺ T cells (**e**), total NK cells, IFN- γ NK cells, and granzyme B⁺ NK cells in the TME (**f**). Data represent mean \pm s.e.m., from a representative experiment ($n = 5$ for PBS or 7 for all other groups (**b**); $n = 8$ (**c**); or $n = 7$ (**d-f**) biologically independent samples) from one (**d**) or three (**b,c,e,f**) independent experiments. *** $P < 0.001$, **** $P < 0.0001$, analysed by one-way (**d**) or two-way (**b,c**) ANOVA with Bonferroni's multiple comparisons test or unpaired two-tailed Student's *t*-test (**e,f**).

number of IFN- γ AH-1-specific CD8⁺ T cells in spleen (Fig. 4f). In contrast, Mann-NC treatment did not increase the frequency of IL-17⁺ CD8⁺ Tc17 cells (Supplementary Fig. 8). Moreover, Mann-NC significantly increased the intra-tumoural frequency of NK cells with elevated expression levels of CD69 and CD107a activation markers (Fig. 4g).

We next studied the role of each immune cell compartment on the anti-tumour efficacy of Mann-NC. Depletion antibodies against CD8⁺ T cells (α CD8), NK cells (α -asialo-GM1), neutrophils (α Ly6G) or isotype control IgG were administered over the course of Mann-NC therapy (Fig. 5a). Depletion antibodies against CD8⁺ T cells or NK cells, but not neutrophils or isotype control, significantly reduced the anti-tumour efficacy of Mann-NC (Fig. 5b). As for the depletion of T_H17 cells, anti-CD4 IgG would non-specifically deplete various subsets of CD4⁺ T cells, including T_H17 cells, T_{reg} cells and other T_H1/T_H2 cells. Thus, we employed anti-IL-17A IgG that neutralizes IL-17A, thereby blocking IL-17-producing effects of T_H17 cells⁴². Administration of anti-IL-17A IgG during the Mann-NC therapy led to significantly reduced anti-tumour efficacy (Fig. 5c). Notably, Mann-NC therapy given without any antigen triggered tumour antigen-specific CD8⁺ and CD4⁺ T-cell responses, as shown by IFN- γ ELISPOT assay with splenocytes restimulated with CT26-derived MHC-I-restricted gp70 AH-1 epitope⁴³ and MHC-II-restricted ME1 neo-epitope⁴⁴, respectively (Fig. 5d). Co-administration of anti-IL-17A IgG during the Mann-NC therapy decreased antigen-specific CD8⁺ and CD4⁺ T-cell responses (Fig. 5d) as well as IFN- γ and granzyme B⁺ activated CD8⁺ T cells and NK cells from the TME (Fig. 5e,f and Extended Data Fig. 4). Collectively, these results show that Mann-NC promotes robust secretion of T_H17-associated cytokines and chemokines, leading to activation and intra-tumoural infiltration of CD8⁺ T cells and NK cells with potent anti-tumour immune response.

α OX40 amplifies the anti-tumour efficacy of Mann-NC

OX40 is a co-stimulatory receptor expressed on activated effector immune cells³¹, and their immune functions can be augmented by

an agonistic antibody against OX40 (α OX40) (ref. 30). As Mann-NC treatment led to marked upregulation of OX40 on CD4⁺ T cells (Fig. 3h), we examined whether co-administration of agonistic α OX40 IgG could further amplify the anti-tumour effects of Mann-NC. CT26 tumour-bearing mice were administered intra-tumourally on days 9, 12 and 15 with either PBS, Mann-NC, α OX40 or Mann-NC + α OX40 combination (Fig. 6a). The Mann-NC + α OX40 combination induced dramatic anti-tumour effects and eliminated established tumours in 88% of mice (Fig. 6b,c). On the other hand, Mann-NC or α OX40 monotherapy slowed the tumour growth but did not lead to tumour eradication. We also tested Mann-NC + α PD-1 IgG combination and found that α PD-1 IgG did not enhance the anti-tumour efficacy of Mann-NC (Supplementary Fig. 9), which is in line with our observation that Mann-NC treatment did not upregulate PD-1 on CD4⁺ T cells (Supplementary Fig. 5b). Survivors from the Mann-NC + α OX40 combination group were protected against CT26 re-challenge performed on day 80 (Fig. 6d), suggesting the establishment of long-term immunological memory. To delineate the combination effect of Mann-NC and α OX40, we performed immune profiling of the TME. Compared with Mann-NC or α OX40 monotherapy, Mann-NC + α OX40 combination therapy further increased the frequency of CD80⁺ DCs and CD8 α ⁺ CD103⁺ CD11c⁺ DCs within the TME (Fig. 7a and Extended Data Fig. 5). Furthermore, T_H17⁺ CD4⁺ T cells induced by Mann-NC treatment were further increased with the Mann-NC + α OX40 combination group, while the frequency of T_{reg} cells remain similar, thus leading to an increased T_H17/T_{reg} ratio in the TME (Fig. 7b). We observed a similar trend of increased T_H17⁺ CD4⁺ T cells in tdLNs with Mann-NC + α OX40 combination (Fig. 7c). Interestingly, whereas α OX40 monotherapy increased T_{reg} cells in tdLNs, Mann-NC monotherapy as well as Mann-NC + α OX40 combination decreased the frequency of T_{reg} cells, resulting in significantly higher T_H17/T_{reg} ratios (Fig. 7c). On the other hand, Mann-NC and/or α OX40 treatment did not change the frequencies of T_H1 or T_H2 cells (Supplementary Fig. 10).

Mann-NC + α OX40 combination also led to potent activation of CD8⁺ T cells and NK cells. Specifically, Mann-NC + α OX40 combination

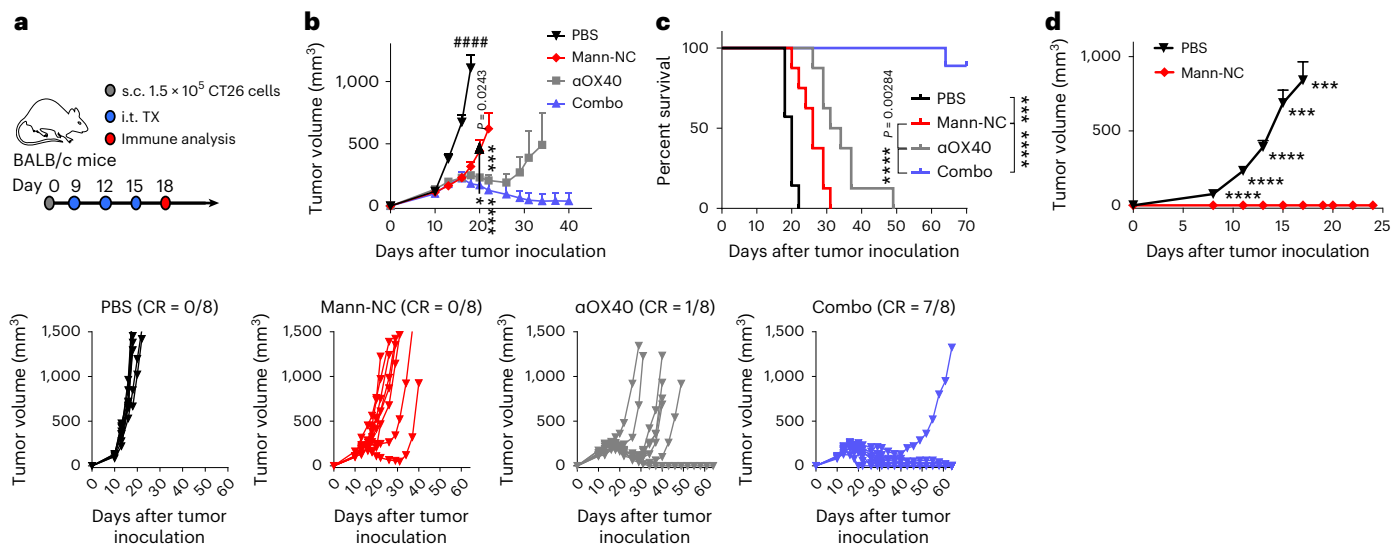


Fig. 6 | Mann-NC and α OX40 combination elicits strong immune activation with potent anti-tumour effect. **a**, BALB/c mice were inoculated subcutaneously (s.c.) with 1.5×10^5 CT26 cells on day 0 and treated by intratumoural (i.t.) administration of Mann-NC and/or α OX40 on days 9, 12 and 15. **b,c**, Average and individual tumour growth (**b**) and survival curves (**c**). CR indicates complete tumor regression. **d**, Survivors were re-challenged with

CT26 cells on day 80. Data represent mean \pm s.e.m., from a representative experiment ($n = 8$ (**b,c**), or $n = 7$ for Mann-NC and 10 for (**d**) biologically independent samples) from three independent experiments (**b,c**). $***P < 0.001$, $****P < 0.0001$, analysed by two-way ANOVA with Bonferroni's multiple comparisons test (**b,d**); or log-rank (Mantel-Cox) test (**c**).

induced high frequencies of intra-tumoural AH-1-tetramer⁺CD8⁺ T cells, with higher levels of IFN- γ ⁺ ($P < 0.01$) and granzyme B⁺ ($P < 0.05$), compared with Mann-NC alone (Fig. 7d). The Mann-NC + α OX40 combination also increased tumour-specific, IFN- γ ⁺ CD8⁺ T cells in tdLN ($P < 0.001$) and spleen ($P < 0.0001$), compared with Mann-NC or α OX40 monotherapy (Fig. 7e,f). Moreover, Mann-NC + α OX40 combination significantly increased the frequency of NK cells with elevated IFN- γ , TNF- α and granzyme B expression (Fig. 7g,h). In addition, Mann-NC + α OX40 combination significantly increased the frequency of CD80⁺ M1-like macrophages ($P < 0.0001$; Fig. 7i), leading to elevated M1/M2 ratio, compared with Mann-NC or α OX40 monotherapy. In line with these results, tumour tissues analysed under confocal microscopy revealed that Mann-NC + α OX40 combination led to robust production of IL-17 and IFN- γ , which co-localized with CD4⁺ and CD8⁺ T cells, respectively (Fig. 7j,k and Extended Data Figs. 6 and 7).

To examine the contributions of T_H17 cells on the anti-tumour efficacy of Mann-NC + α OX40 combination, we co-administered anti-IL-17A IgG during Mann-NC + α OX40 combination treatment; this resulted in significantly diminished anti-tumour effects ($P < 0.0001$; Fig. 8a), thus showing the anti-tumour effects of IL-17-producing T_H17 cells. Furthermore, we assessed abscopal effects of Mann-NC + α OX40 combination using a bilateral CT26 tumour model, where only the primary tumours received treatments (Fig. 8b). Mann-NC + α OX40 combination effectively inhibited the growth of treated, primary tumours, as well as untreated, contralateral tumours (Fig. 8b), demonstrating systemic anti-tumour efficacy of local Mann-NC + α OX40 combination therapy.

Lastly, we sought to validate the anti-tumour effect of the Mann-NC + α OX40 combination in other tumour models. In C57BL/6 mice bearing MC38 colon carcinoma, the Mann-NC + α OX40 combination therapy eradicated tumours in 100% of the animals, whereas Mann-NC alone or α OX40 monotherapy exhibited modest anti-tumour effects ($P < 0.01$; Fig. 8c,d). Moreover, we observed strong anti-tumour efficacy of Mann-NC + α OX40 combination therapy in the B16F10 melanoma model as well as in the tobacco-associated head-and-neck cancer model of NOOC1 tumour that we recently developed (Fig. 8e,f)⁴⁵. On the other hand, intra-tumoural administration of LPS with or without α OX40 did not show anti-tumour effects in the CT26

tumour model (Supplementary Fig. 11). Collectively, these results show that the Mann-NC + α OX40 combination potently activates DCs, macrophages, T_H17 cells, CD8⁺ T cells and NK cells, and that it exerts robust anti-tumour efficacy.

In summary, we have developed a pathogen-mimetic 'nano-PAMP' based on polysaccharide mannan, and presented an approach for exploiting pathogen-associated T_H17 immunity to improve cancer immunotherapy. Mann-NC with hollow capsule morphology and the surface display of PAMPs mimics the yeast cell wall in nanoscale dimension (Fig. 1). Mann-NC endocytosed by DCs activates the Dectin-2 and TLR-4 signalling pathways (Fig. 2a–i), leading to the selective expansion of T_H17 cells without triggering T_H1, T_H2 or Tc17 responses, and the release of pro-inflammatory cytokines and chemokines, including IL-17, IL-23 and CXCL10 within the TME (Figs. 2j–l, 3i and 4a–d). These immunological changes in the TME promoted tumour infiltration of activated CD8⁺ T cells and NK cells, resulting in increased ratios of T_H17 cells:T_{reg} cells, CD8⁺ T cells:T_{reg} cells, and M1/M2 macrophages (Figs. 3g,k and 4e–g). Moreover, by combining Mann-NC with α OX40 IgG, we further amplified T_H17-driven anti-tumour immune responses and achieved robust anti-tumour efficacy in multiple murine tumour models (Figs. 6–8). Overall, our study provides a biomaterial-based strategy for tipping the balance between T_H17 cells and T_{reg} cells in the TME and for exploiting T_H17-based immune activation for orchestrating immune responses.

Methods

Reagents and instruments

Mannan from *S. cerevisiae*, triethylamine, ammonium fluoride and PEI (branched, molecular weight 25,000) were purchased from Sigma-Aldrich. siNPs (approximately 200 nm in diameter, 10 mg ml⁻¹ in water) were purchased from nanoComposix. Amine-modified cyanine5.5 was obtained from Lumiprobe. Sodium meta-periodate and dimethyl 3,3'-dithiobispropionimidate \cdot 2HCl (DTBP) were obtained from Thermo Fisher Scientific. UV-Vis absorption and fluorescence were measured using BioTek Synergy Neo microplate reader. TEM images were acquired using JEOL 1400-plus, and AFM was performed using Asylum-1 MFP-3D. Hydrodynamic size and zeta potential measurement were performed using Malvern Zetasizer Nano ZSP.

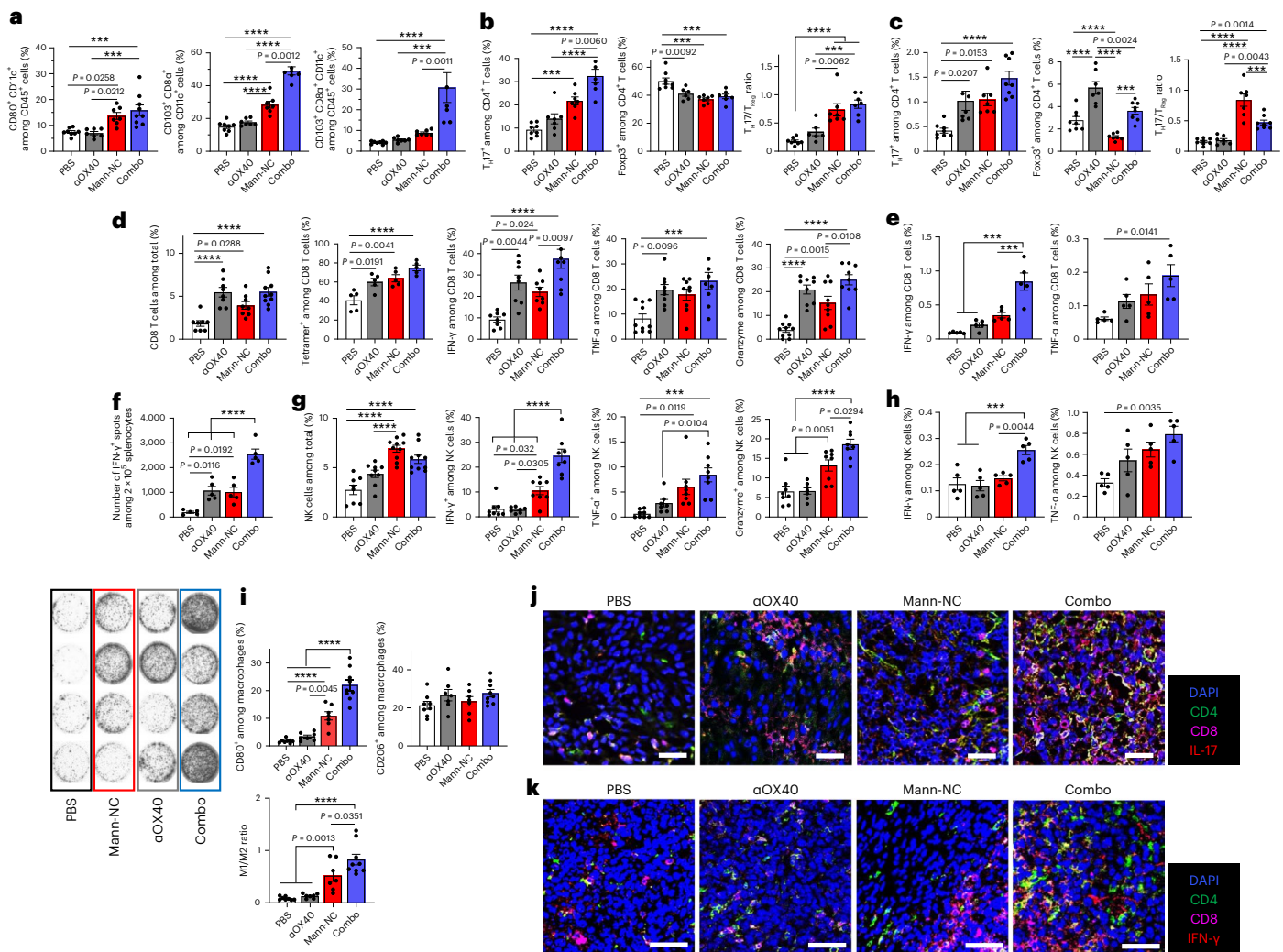


Fig. 7 | Mann-NC and α OX40 combination elicits strong immune activation with potent anti-tumour effect. BALB/c mice were inoculated subcutaneously with 1.5×10^5 CT26 cells on day 0 and treated by intra-tumoural administration of Mann-NC and/or α OX40 on days 9, 12 and 15. **a**, Intra-tumoural frequencies of CD80⁺ CD11c⁺ DCs and CD8 α ⁺ CD103⁺ CD11c⁺ DCs. **b, c**, Frequencies of IL-17⁺ CD4⁺ T_H17 cells, Foxp3⁺ CD4⁺ T_H17 cells and the corresponding T_H17/T_{reg} ratio within the TME (**b**) and tDLNs (**c**). **d, e**, Frequencies, tetramer staining and intracellular cytokine profiles of CD8⁺ T cells within the TME (**d**) and tDLNs (**e**). **f**, IFN- γ ⁺ ELISPOT analysis of splenocytes after restimulation with AH-1 peptide.

g, h, Frequencies and intracellular cytokine profiles of NK cells within the TME (**g**) and tDLNs (**h**). **i**, Intra-tumoural frequencies of CD80⁺ M1- and CD206⁺ M2-like macrophages and the corresponding M1/M2 ratio. **j, k**, Confocal microscopic images of tumour tissues excised on day 15 and stained with the indicated antibodies. Data represent mean \pm s.e.m., from a representative experiment ($n = 7$ for PBS or 8 for α OX40, Mann-NC and the combination (**a–d, f, g, i**), $n = 5$ (**e, h, j, k**) biologically independent samples) from two (**j, k**) or three (**a–i**) independent experiments. *** $P < 0.001$, **** $P < 0.0001$, analysed by one-way (a–i) ANOVA with Bonferroni's multiple comparisons test. Scale bars, 50 μ m (**j, k**).

Flow cytometry analyses were performed using Ze5 (Beckman Coulter), and the data were analysed using FlowJo 10.2 software. Confocal microscopy images were taken with Leica SP8 confocal microscope and analysed by ImageJ software (V 1.8.0).

Synthesis and characterization of Mann-NC

Mannan polymer (Mann) was first chemically modified to generate amine-reactive, aldehyde functional group by oxidation of hydroxyl groups. In detail, 200 μ g of Mann was dissolved in 6 ml of ultrapure water and mixed with 6 ml of 0.01 M sodium periodate solution and reacted for 1 h with gentle shaking at room temperature in the dark. The product was purified using dialysis (molecular weight cut-off 1,000 Da, Spectrum) against de-ionized water for 3 days and lyophilized by freeze-drying in the dark for 2–3 days. The resulting aldehyde-modified Mann (Mann-CHO) was characterized using a modified hydroxylamine hydrochloride method⁴⁶ for the aldehyde content and kept at 4 $^{\circ}$ C in the dark until further use.

Mann-NC was constructed using siNPs as a sacrificing template. Briefly, siNP (15 mg in 900 μ l) was added with 15 μ l of aqueous PEI25K solution (100 mg ml⁻¹) and incubated for 10 min with vigorous vortex. The resulting PEI-siNP was centrifuged three times to remove excessive PEI25K, further reacted with bioreducible DTBP (0.5 mg in 1 ml 0.1 M triethylamine buffer at pH 8) for 1 h at room temperature to crosslink surface PEI, and then washed three times with ultrapure water. The outermost surface of crosslinked PEI-siNP was incubated with Mann-CHO (1,000 μ l, 2 mg ml⁻¹ ultrapure water) for 12 h at room temperature to prepare Mann-coated siNP. Finally, Mann-NC was obtained by selectively dissolving the solid siNP core using ammonium fluoride, followed by successive washing with ultrapure water three times and PBS twice. Hydrodynamic size and zeta potential of Mann-NC were measured using Malvern Zetasizer Nano ZS. Mann-NC (5 mg ml⁻¹ in PBS) was stored at 4 $^{\circ}$ C until further use. The endotoxin level for each in vivo dose of Mann-NC and native Mann was measured to be <0.05 endotoxin units (EU) per dose, as determined by the LAL Chromogenic Endotoxin Quantitation Kit (Pierce).

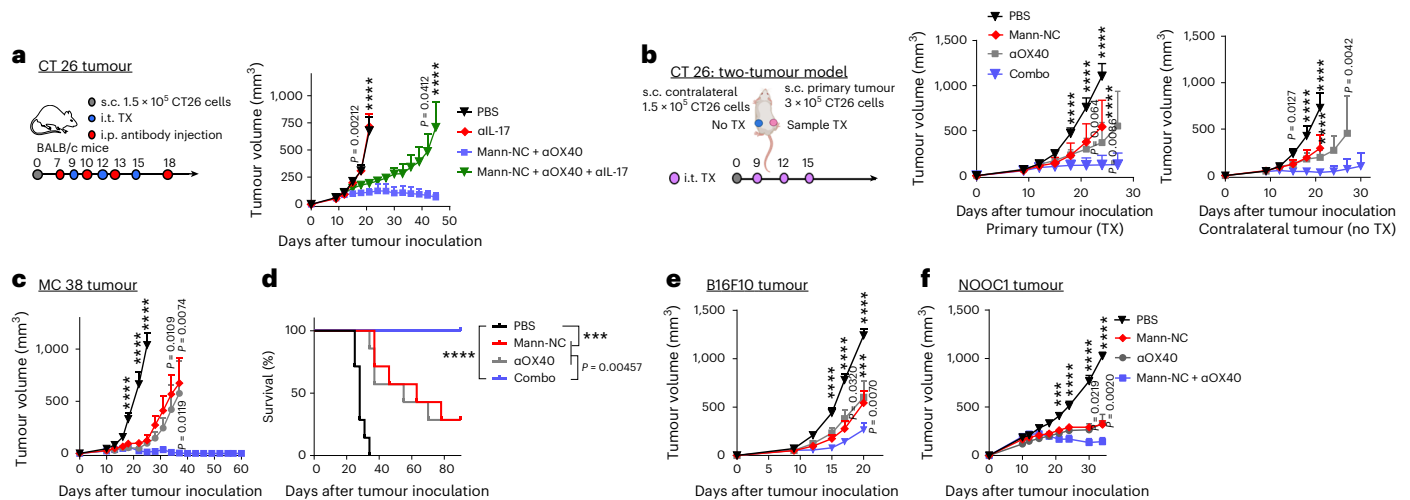


Fig. 8 | Mann-NC and α OX40 combination exhibits robust anti-tumour efficacy in murine tumour models. **a**, BALB/c mice were inoculated subcutaneously (s.c.) with 1.5×10^5 CT26 cells on day 0 and treated by intratumoural (i.t.) administration of Mann-NC and α OX40 on days 9, 12 and 15. A subset of animals received intraperitoneal (i.p.) administration of anti-IL-17A on days 7, 10, 13 and 18, followed by monitoring of tumour growth. **b**, BALB/c mice were inoculated subcutaneously with 3×10^5 CT26 cells on the right flank and 1.5×10^5 CT26 cells on the left flank on day 0, and samples were administered only into the right, primary tumours on days 9, 12 and 15. Shown are the average growth of primary and contralateral tumours. **c,d**, C57BL/6 mice were inoculated subcutaneously with 6×10^5 MC38 cells on day 0 and

treated by intra-tumoural administration of Mann-NC and/or α OX40 on days 9, 12 and 15. Average tumour growth (**c**) and animal survival (**d**). **e,f**, C57BL/6 mice were inoculated subcutaneously with 2×10^5 B16F10 melanoma cells (**e**) or 2×10^6 NOOC1 head and neck cancer cells (**f**) on day 0. The treatments were given intra-tumourally starting day 8 for the B16F10 melanoma model and day 10 for the NOOC1 model with five injections 3 days apart. Data represent mean \pm s.e.m., from a representative experiment ($n = 7$ (**e,f**) or 8 (**a-d**) biologically independent samples) from one (**e**) or two (**a-d,f**) independent experiments. *** $P < 0.001$, **** $P < 0.0001$, analysed by two-way ANOVA with Bonferroni's multiple comparisons test (**a-c,e-f**); or log-rank (Mantel-Cox) test (**d**).

Mann-NC uptake studies with BMDCs

BMDCs were prepared according to the literature⁴⁷. Briefly, aseptically isolated bone-marrow cells from femurs and tibia of C57BL/6 mice were cultured in complete DC medium (RPMI-1640 (Gibco) supplemented with 10% foetal bovine serum (FBS, Corning), 1% penicillin-streptomycin (Gibco), 55 μ M β -mercaptoethanol (Gibco) and 20 ng ml⁻¹ granulocyte-macrophage colony-stimulating factor (GenScript)) at 37 °C with 5% CO₂. Fresh medium was supplemented on day 3, and the medium was replaced on days 6 and 8. The cultured BMDCs were used between days 7 and 12 before being fully matured.

For time-dependent uptake study, immature BMDCs in complete DC medium were plated at 10^5 cells per well in 96-well round-bottom plate and cultured 12 h with the Mann-NC or Native-Mann for the indicated duration. For the Mann-NC uptake inhibition studies, BMDCs were pre-treated for 30 min with 20 μ l of pharmacological inhibitors, including dextran sulfate (4 mg ml⁻¹), chlorpromazine (50 μ M), cytochalasin D (2.5 μ M) and M β -CD (32 μ M). BMDCs were then collected with cell dissociation reagent (StemPro Accutase, Gibco) and washed twice with PBS for flow cytometry analysis. For antibody staining, BMDCs were treated with anti-CD16/32 Fc γ blocking antibody (eBioscience) in 1:20 dilution for 10 min and further stained with anti-CD11c antibody (eBioscience) in 1:100 dilution for 30 min at room temperature. After washing twice with FACS buffer (1% BSA in PBS), cells were dispersed in FACS buffer with 4,6-diamidino-2-phenylindole (DAPI, 300 nM) for running flow cytometry. For confocal microscopy analysis, 3×10^5 BMDCs were plated on the coverslip-bottom 12-well plate and treated for 6 h with Mann-NC or Native-Mann prepared using Cy5.5-conjugated mannan. BMDCs were then washed three times with cold PBS, stained with DAPI in PBS (300 nM) for 30 min, and fixed with 4% formaldehyde for 30 min. After mounting coverslips with a mounting medium (Molecular Probes), cells were imaged by a confocal microscope.

BMDC activation and cytokine release

A total of 10^5 BMDCs were plated per well in 96-well round-bottom plate and treated for 12 h with Native-Mann or Mann-NC. Supernatants were collected for cytokine analysis, including IL-12p70, TNF- α and IL-6, while BMDCs were stained with anti-CD16/32 blocking antibody in 1:20 dilution for 10 min, followed by fluorophore-labelled antibodies in 1:100 dilution for 30 min against CD11c (FITC, eBioscience), CD40 (PE, eBioscience), CD86 (APC, eBioscience) and MHC-II (PE-CY7, BioLegend). Cells were analysed by flow cytometry.

PRR inhibition study using blocking antibodies

A total of 10^5 BMDCs were seeded on 24-well plate and incubated for 30 min with blocking antibodies (2 μ g ml⁻¹) against PRRs on BMDCs surface, including Dectin-1, Dectin-2, CD206, CD209 (DC-SIGN), Mincle, TLR-2 and TLR-4, followed by treatment with Native-Mann or Mann-NC for 12 h. Supernatants were collected for TNF- α analysis by enzyme-linked immunosorbent assay (ELISA; R&D system).

Incubation with HEK-blue Dectin and TLR cells

A total of 2×10^5 HEK-blue cells (Dectin-1, Dectin-2, TLR-2 and TLR-4 cells from Invivogen) were incubated with Mann formulations in HEK-blue detection medium. Zymosan, and LPS (1 μ g ml⁻¹) were employed as positive controls for Dectin-1/2, TLR-2 and TLR-4, respectively. Activation of HEK-blue cells was quantified after 12 h by the absorbance at 650 nm.

In vitro CD4⁺ T-cell differentiation

T_H1, T_H2, iT_{reg} and T_H17 cells were generated by activating naive CD4⁺ T cells with anti-CD3 and anti-CD28 monoclonal antibodies in the presence of cytokines and neutralizing antibodies. Briefly, naive CD4⁺ T cells were isolated from spleen and lymph nodes using naive CD4⁺ T-cell isolation kit (STEMCELL Technology) according to the manufacturer's protocol. Isolated naive CD4⁺ T cells were then resuspended

in conditioned BMDC medium obtained by incubating BMDCs with Mann-NC or Native-Mann for 12 h, and stimulated for 3–5 days with pre-coated anti-CD3 ($1 \mu\text{g ml}^{-1}$, BioLegend) and anti-CD28 ($1 \mu\text{g ml}^{-1}$, BioLegend) in 96-well plate.

For ICS by flow cytometry, cells were restimulated with PMA (10 ng ml^{-1}) and ionomycin ($1,000 \text{ ng ml}^{-1}$) for 4 h in the presence of Brefeldin A ($5 \mu\text{g ml}^{-1}$). After washing twice with FACS buffer, antibody staining was performed in 1:100 dilution against surface markers CD4⁺ (APC) and CD25 (BV605), followed by lineage-specific, intracellular cytokine staining after fixation and permeabilization; IFN- γ (PE-CY7), IL-4 (BV605), Foxp3 (PE) and IL-17 (FITC). Supernatant collected from each well was analysed for cytokines by ELISA.

BMDC and BDC2.5 CD4⁺ T-cell co-culture studies

A total of 10^5 BMDCs isolated from BDC2.5 transgenic mice were seeded on 96-well plate and treated overnight with 100 ng of MHC-II-restricted p31 epitope (the cognate antigen for BDC2.5 transgenic CD4⁺ T cells) in the presence or absence of Mann-NC. BDC2.5 CD4⁺ T cells were isolated from spleen and lymph nodes of BDC2.5 T cell receptor transgenic mice using CD4⁺ T-cell isolation kit and added to p31-pulsed BMDCs (2×10^4 cells per well). After 3 days, CD4⁺ T cells were analysed by ICS as described above, and the cell medium from each well was analysed for IL-17A by ELISA.

Flow cytometry and antibodies

Single-cell suspensions were incubated with Fc receptor-blocking anti-CD16/32 antibody (eBioscience) at room temperature for 10 min, and stained with Fixable viability Dye eFluor 450 (eBioscience) at 37 °C for 30 min. After washing, surface markers were stained for 30 min at 4 °C. To detect cytokine production upon ex vivo restimulation, cells were resuspended in RPMI-1640 with 10% FBS and then cultured on plates pre-coated with $1 \mu\text{g ml}^{-1}$ anti-CD3 antibody (clone 145-2C11; BioLegend) and $1 \mu\text{g ml}^{-1}$ anti-CD28 antibody (clone 37.51; BioLegend) for 5 h at 37 °C in the presence of $2.5 \mu\text{g ml}^{-1}$ Brefeldin A Solution (BioLegend). Cells were processed for intracellular cytokine staining as described above.

Animal experiments

Animals were cared for following the federal, state, and local guidelines. All work performed on animals was in accordance with and approved by the Institutional Animal Care and Use Committee at the University of Michigan, Ann Arbor. For in vivo studies, 6–8-week-old female BALB/c mice (Jackson Laboratory, 18–20 g) and C57BL/6 mice (Jackson Laboratory, 18–20 g) were used. NOD.BDC2.5 transgenic mice (5–7-week-old female or male, 15–20 g) were obtained from Jackson Laboratory. Mice were housed in 12 h light–dark cycle, at 72 F, and about 30% humidity. For studies with CT26 colon carcinoma, BALB/c mice were subcutaneously inoculated on the right flank with 1.5×10^5 CT26 cells on day 0 and administered with samples on days 9, 12 and 15 by intra-tumoural injection. The dose of mannan-based formulations (Native-Mann and Mann-NC) were matched at 1 mg mannan per injection. For the combination study, anti-mouse OX40 (5 or 20 μg per injection) was co-administered with Mann-NC via intra-tumoural (i.t.) route on days 9, 12 and 15. After 80 days of the tumour inoculation, surviving mice were re-challenged with 5×10^5 CT26 cells on the left flank to evaluate immunological memory effect. For the antibody depletion study, depletion antibodies (200 μg per injection) against CD8 α (BioXcell, clone 2.43, #BP0061), CD4 (BioXcell, clone GK1.5, #BP0003-1), NK (Wako chemicals USA, anti-asialo GM1, #986-10001), Ly6G (BioXcell, clone 1A8, #BP0075-1), IL-17A (BioXcell, clone 17F3, #BE0173) and isotype control immunoglobulin G 2b (BioXcell, clone LTF-2, #BP0090) were administered intraperitoneally on days 7, 10, 13 and 18. For combination studies in MC38 colon carcinoma model, C57BL/6 mice were subcutaneously inoculated with 5×10^5 MC38 cells on the right flank on day 0, followed by i.t. administration of Mann-NC and/or α OX40 (20 μg per injection) on days 9, 12 and 15.

For the therapeutic studies, C57BL/6 mice were inoculated with 1×10^5 B16F10 cells (ATCC) per mouse on the right flank by subcutaneous injection on day 0 and treated on the indicated days. Immune checkpoint blocker-resistant NOOC1 head-and-neck cells were maintained as reported previously⁴⁵ in Iscove's modified Dulbecco's medium (Gibco, 12440053) supplemented with with F-12 nutrient mix (Gibco, 11765054), FBS (Hyclone, SH3039603), penicillin–streptomycin (Thermo Fisher, 15-140-122), insulin (Invitrogen, 12585014), hydrocortisone (Sigma-Aldrich, H0888-1G) and epidermal growth factor (EMD Millipore, 01-107). For in vivo inoculation, NOOC1 was washed once with PBS and mixed with Matrigel (Thermo Fisher, CB-40230) to reach the cell density of 2×10^7 cells ml^{-1} . A total of 2×10^6 NOOC1 cells were implanted on the right flank of each mouse. Tumour growth was monitored every other day, and the tumour volume was calculated by $(\text{width})^2 \times \text{length} \times 0.52$. Animals were killed when the tumour masses reached 1.5 cm in one dimension or when animals became moribund or exhibited severe weight loss or tumour ulceration.

ELISPOT

For analysis of tumour antigen-specific CD8 α^+ T-cell response, ELISPOT assay was performed with splenocytes from immunized mice. Spleens were collected aseptically, processed into single-cell suspension, and plated with 5×10^5 splenocytes per well in 96-well PVDF plates (EMD Millipore) pre-coated with IFN- γ antibody (R&D Systems) overnight. Splenocytes were then restimulated with antigen peptides ($2 \mu\text{g ml}^{-1}$) or controls for 24 h. Assays were completed using sequential incubations with biotinylated secondary antibody, streptavidin alkaline phosphatase (Sigma Chemical) and NBT/BCIP substrate (Surmodics). Developed spots were analysed using an AID iSpot Reader (Autoimmun Diagnostika GmbH).

Tissue processing and cell staining for flow cytometry

Tumours and tumour draining LNs were excised and homogenized using pestle motor and treated with collagenase type IV (Sigma-Aldrich, 1 mg ml^{-1}) and DNase I (Sigma-Aldrich, 100 U ml^{-1}) in 1 ml of serum-free RPMI medium for 30 min at 37 °C with gentle shaking. For cytokine/chemokine analysis, supernatants were collected and kept at -70 °C. The cell suspension was then filtered through a cell strainer (70 μm) and washed with FACS buffer three times. Cells were incubated with CD16/32 blocking antibody in 1:20 dilution for 10 min, and then stained with antibodies for 30 min at room temperature. For the TME analysis, CD8, CD4, NK cells, DCs, monocytes, MDSCs and macrophages were stained with the following antibodies in 1:100 dilution: CD8⁺ T cells (CD45-FITC, CD8 α -APC and CD3-PE-CY7), CD4⁺ T cells (CD45-FITC, CD4-APC and CD3-PE-CY7), DCs (CD45-FITC, CD11c-PE and CD86-PE-CY7), NK cells (CD45-FITC, CD49b-PE and CD3-PE-CY7), MDSCs (Ly6G-PE, Ly6C-APC and CD11b-FITC) and others (Dectin-2/CLEC6A α -APC and CD284 (TLR-4)-PE). Cells were washed twice with FACS buffer, resuspended in $2 \mu\text{g ml}^{-1}$ DAPI solution, and analysed by flow cytometry.

Immunofluorescence staining

For immunofluorescence staining, tumour tissues were excised and cut into small pieces. Tumour tissues were embedded in OCT compound and flash-frozen in liquid nitrogen. The frozen blocks were sectioned into 6 μm thickness and attached to slide glasses. Sectioned tumours were kept in room temperature for 10 min and washed with DPBS. Washed tissue sections were permeabilized with 0.3% Triton X100 in PBS (PBS-T) for 1 h, and blocked with 1% BSA in PBST for 1 h. Tissue sections were stained at 4 °C for 24 h with primary antibodies diluted to 1:100 in 1% BSA–PBST, followed by staining at room temperature for 2 h with fluorophore-conjugated secondary antibodies diluted to 1:500 in 1% BSA–PBST. CD8⁺ and CD4⁺ T cells were stained with the following antibodies: primary antibodies (CD3 (R&D Systems, #MAB4841-100), IFN- γ (R&D Systems, #AF-585-NA), IL-17A (R&D Systems, #AF-421-NA),

integrin $\alpha 2/CD49b$ (R&D Systems, #AF1740), CD4 (Novus Biologicals, #NBPI-19371), CD8 (Novus Biologicals, #NBPI-49045); secondary antibodies (goat anti-rabbit IgG H&L (Alexa Flour 488, Abcam, #ab150077), donkey anti-sheep IgG H&L (Alexa Flour 488, Abcam, #ab150177), donkey anti-goat IgG H&L (Cy3, Abcam, #ab6949) and goat anti-rat IgG H&L (Alexa Flour 647, Invitrogen, #A-21247)). Then, the tissue sections were stained with DAPI and mounted on slide glass using Prolong Diamond Antifade mountant (Invitrogen). Stained tumours were analysed with confocal microscopy (Nikon A1RSi).

Statistical analysis

Sample sizes were chosen on the basis of preliminary data from pilot experiments and previously published results in the literature. All animal studies were performed after randomization. Experiments were not performed in a blinded fashion. Statistical analysis was performed with Prism 6.0 software (GraphPad Software) by one-way or two-way analysis of variance (ANOVA) with Bonferroni multiple comparisons post-test. Statistical significance for the survival curve was calculated by the log-rank test. Data were approximately normally distributed, and variance between groups was similar. Statistical significance was indicated as * $P < 0.05$, ** $P < 0.01$, *** $P < 0.001$ and **** $P < 0.0001$.

Reporting summary

Further information on research design is available in the Nature Portfolio Reporting Summary linked to this article.

Data availability

The main data supporting the results in this study are available within the paper and its Supplementary Information. Source data are provided with this paper. All data generated in this study are available from the corresponding authors on reasonable request.

References

- Medzhitov, R. & Janeway, C. Jr Innate immunity. *N. Engl. J. Med* **343**, 338–344 (2000).
- Matzinger, P. The danger model: a renewed sense of self. *Science* **296**, 301–305 (2002).
- Mogensen, T. H. Pathogen recognition and inflammatory signaling in innate immune defenses. *Clin. Microbiol. Rev.* **22**, 240–273 (2009).
- Zou, W. & Restifo, N. P. T_H17 cells in tumour immunity and immunotherapy. *Nat. Rev. Immunol.* **10**, 248–256 (2010).
- Noack, M. & Miossec, P. T_H17 and regulatory T cell balance in autoimmune and inflammatory diseases. *Autoimmun. Rev.* **13**, 668–677 (2014).
- Khader, S. A. et al. IL-23 and IL-17 in the establishment of protective pulmonary $CD4^+$ T cell responses after vaccination and during *Mycobacterium tuberculosis* challenge. *Nat. Immunol.* **8**, 369–377 (2007).
- Bettelli, E., Korn, T., Oukka, M. & Kuchroo, V. K. Induction and effector functions of T_H17 cells. *Nature* **453**, 1051–1057 (2008).
- Quintana, F. J. et al. Control of T_{reg} and T_H17 cell differentiation by the aryl hydrocarbon receptor. *Nature* **453**, 65–71 (2008).
- Korn, T., Bettelli, E., Oukka, M. & Kuchroo, V. K. IL-17 and T_H17 cells. *Annu. Rev. Immunol.* **27**, 485–517 (2009).
- Solt, L. A. et al. Suppression of T_H17 differentiation and autoimmunity by a synthetic ROR ligand. *Nature* **472**, 491–494 (2011).
- Esplugues, E. et al. Control of T_H17 cells occurs in the small intestine. *Nature* **475**, 514–518 (2011).
- Xu, T. et al. Metabolic control of T_H17 and induced T_{reg} cell balance by an epigenetic mechanism. *Nature* **548**, 228–233 (2017).
- Hang, S. et al. Bile acid metabolites control T_H17 and T_{reg} cell differentiation. *Nature* **576**, 143–148 (2019).
- Wilke, C. M., Bishop, K., Fox, D. & Zou, W. Deciphering the role of T_H17 cells in human disease. *Trends Immunol.* **32**, 603–611 (2011).
- Knochelmann, H. M. et al. When worlds collide: T_H17 and T_{reg} cells in cancer and autoimmunity. *Cell. Mol. Immunol.* **15**, 458–469 (2018).
- Martin-Orozco, N. et al. T helper 17 cells promote cytotoxic T cell activation in tumor immunity. *Immunity* **31**, 787–798 (2009).
- Kryczek, I. et al. Phenotype, distribution, generation, and functional and clinical relevance of T_H17 cells in the human tumor environments. *Blood* **114**, 1141–1149 (2009).
- Xie, Y. et al. Naive tumor-specific $CD4^+$ T cells differentiated in vivo eradicate established melanoma. *J. Exp. Med.* **207**, 651–667 (2010).
- Muranski, P. et al. T_H17 cells are long lived and retain a stem cell-like molecular signature. *Immunity* **35**, 972–985 (2011).
- Viaud, S. et al. Cyclophosphamide induces differentiation of T_H17 cells in cancer patients. *Cancer Res.* **71**, 661–665 (2011).
- Si, Y. et al. Adjuvant-free nanofiber vaccine induces in situ lung dendritic cell activation and T_H17 responses. *Sci. Adv.* **6**, eaba0995 (2020).
- Robinson, M. J. et al. Dectin-2 is a Syk-coupled pattern recognition receptor crucial for T_H17 responses to fungal infection. *J. Exp. Med.* **206**, 2037–2051 (2009).
- Saijo, S. et al. Dectin-2 recognition of α -mannans and induction of T_H17 cell differentiation is essential for host defense against *Candida albicans*. *Immunity* **32**, 681–691 (2010).
- Netea, M. G. et al. Variable recognition of *Candida albicans* strains by TLR4 and lectin recognition receptors. *Med Mycol.* **48**, 897–903 (2010).
- Kawai, T. & Akira, S. The role of pattern-recognition receptors in innate immunity: update on Toll-like receptors. *Nat. Immunol.* **11**, 373 (2010).
- Garcia-Rubio, R., de Oliveira, H. C., Rivera, J. & Trevijano-Contador, N. The fungal cell wall: *Candida*, *Cryptococcus*, and *Aspergillus* species. *Front. Microbiol.* **10**, 2993 (2019).
- Son, S. et al. Sugar-nanocapsules imprinted with microbial molecular patterns for mRNA vaccination. *Nano Lett.* **20**, 1499–1509 (2020).
- Pradhan, A. et al. Non-canonical signalling mediates changes in fungal cell wall PAMPs that drive immune evasion. *Nat. Commun.* **10**, 5315 (2019).
- Graus, M. S. et al. Mannan molecular substructures control nanoscale glucan exposure in *Candida*. *Cell Rep.* **24**, 2432–2442. e2435 (2018).
- Croft, M. Control of immunity by the TNFR-related molecule OX40 (CD134). *Annu. Rev. Immunol.* **28**, 57–78 (2010).
- Aspeshlagh, S. et al. Rationale for anti-OX40 cancer immunotherapy. *Eur. J. Cancer* **52**, 50–66 (2016).
- Korolenko, T. A., Bgatova, N. P. & Vetvicka, V. Glucan and mannan—two peas in a pod. *Int. J. Mol. Sci.* **20**, 3189 (2019).
- Vendele, I. et al. Mannan detecting C-type lectin receptor probes recognise immune epitopes with diverse chemical, spatial and phylogenetic heterogeneity in fungal cell walls. *PLoS Pathog.* **16**, e1007927 (2020).
- Hou, Y. et al. Co-delivery of antigen and dual adjuvants by aluminum hydroxide nanoparticles for enhanced immune responses. *J. Control. Release* **326**, 120–130 (2020).
- Rennick, J. J., Johnston, A. P. & Parton, R. G. Key principles and methods for studying the endocytosis of biological and nanoparticle therapeutics. *Nat. Nanotechnol.* **16**, 266–276 (2021).
- Chen, C. & Gao, F.-H. T_H17 cells paradoxical roles in melanoma and potential application in immunotherapy. *Front. Immunol.* **10**, 187 (2019).
- Ankathatti Munegowda, M., Deng, Y., Mulligan, S. J. & Xiang, J. T_H17 and T_H17 -stimulated $CD8^+$ T cells play a distinct role in T_H17 -induced preventive and therapeutic antitumor immunity. *Cancer Immunol. Immunother.* **60**, 1473–1484 (2011).

38. Shortman, K. & Heath, W. R. The CD8⁺ dendritic cell subset. *Immunological Rev.* **234**, 18–31 (2010).
39. Cerovic, V. et al. Lymph-borne CD8⁺ dendritic cells are uniquely able to cross-prime CD8⁺ T cells with antigen acquired from intestinal epithelial cells. *Mucosal Immunol.* **8**, 38–48 (2015).
40. McGeachy, M. J. et al. The interleukin 23 receptor is essential for the terminal differentiation of interleukin 17-producing effector T helper cells in vivo. *Nat. Immunol.* **10**, 314–324 (2009).
41. Bromley, S. K., Mempel, T. R. & Luster, A. D. Orchestrating the orchestrators: chemokines in control of T cell traffic. *Nat. Immunol.* **9**, 970–980 (2008).
42. Xin, L. et al. Commensal microbes drive intestinal inflammation by IL-17-producing CD4⁺ T cells through ICOSL and OX40L costimulation in the absence of B7-1 and B7-2. *Proc. Natl Acad. Sci. USA* **111**, 10672–10677 (2014).
43. Huang, A. Y. et al. The immunodominant major histocompatibility complex class I-restricted antigen of a murine colon tumor derives from an endogenous retroviral gene product. *Proc. Natl Acad. Sci. USA* **93**, 9730–9735 (1996).
44. Kreiter, S. et al. Mutant MHC class II epitopes drive therapeutic immune responses to cancer. *Nature* **520**, 692–696 (2015).
45. Sun, X. et al. Amplifying STING activation by cyclic dinucleotide-manganese particles for local and systemic cancer metalloimmunotherapy. *Nat. Nanotechnol.* **16**, 1260–1270 (2021).
46. Zhao, H. & Heindel, N. D. Determination of degree of substitution of formyl groups in polyaldehyde dextran by the hydroxylamine hydrochloride method. *Pharm. Res.* **8**, 400–402 (1991).
47. Lutz, M. B. et al. An advanced culture method for generating large quantities of highly pure dendritic cells from mouse bone marrow. *J. Immunol. Methods* **223**, 77–92 (1999).

Acknowledgements

This work was supported in part by NIH (R01DE030691, R01DE031951, R01DK125087, R01CA271799, R01NS122536, U01CA210152 and P30CA046592), David Koch-Prostate Cancer Foundation Award in Nanotherapeutics and National Research Foundation of Korea (NRF) grant funded by the Korean government (MSIT) (2022R1F1A1075064 and 2022R1A2C1006643). A.S.K. acknowledges financial support from the UM CBTP Training Program (NIH T32GM008353). K.S.P. acknowledges financial support from the UM TEAM Training Program (NIH T32DE007057). We thank the NIH Tetramer Core Facility (contract HHSN272201300006C) for provision of MHC-I tetramers; and the University of Michigan Cancer Center Immunology Core for ELISA analysis.

Author contributions

S.S., J.N. and J.J.M. designed the study. S.S., J.N., A.S.K., K.S.P., M.T.P., J.A. and B.S. performed the experiments. S.S., J.N., W.Z., S.-H.L., J.S., O.C.F. and J.J.M. interpreted the data. S.S., J.N. and J.J.M. wrote the paper.

Competing interests

A patent application for particles for the delivery of biomolecules has been filed, with S.S., O.C.F. and J.J.M. as inventors. O.C.F. has financial interests in Selecta Biosciences, Tarveda Therapeutics, and Seer. J.J.M. declares financial interests for board membership, as a paid consultant, for research funding, and/or as equity holder in EVOQ Therapeutics, Saros Therapeutics and Intrinsic Medicine.

Additional information

Extended data is available for this paper at <https://doi.org/10.1038/s41551-022-00973-4>.

Supplementary information The online version contains supplementary material available at <https://doi.org/10.1038/s41551-022-00973-4>.

Correspondence and requests for materials should be addressed to Sejin Son or James J. Moon.

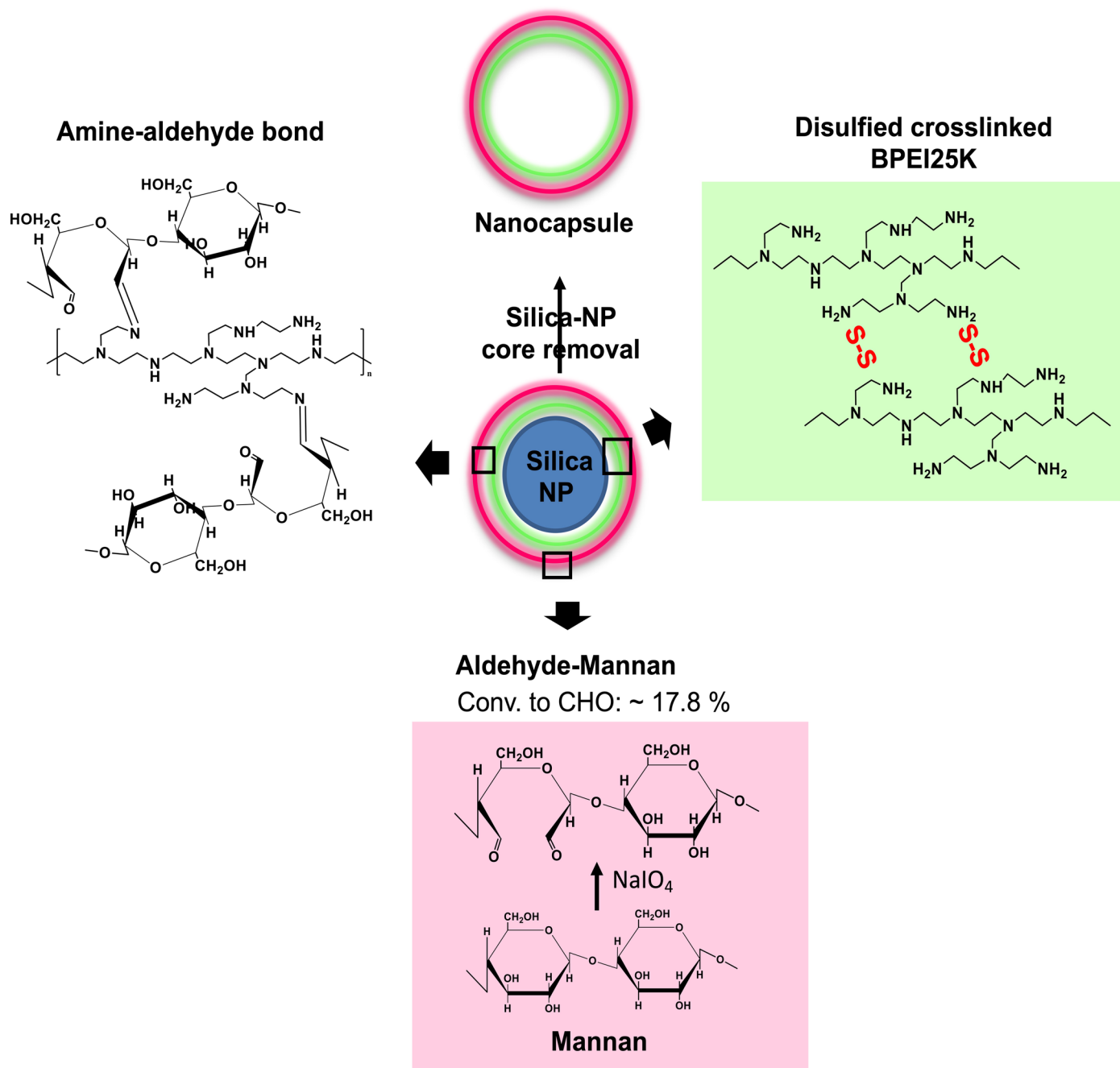
Peer review information *Nature Biomedical Engineering* thanks Miodrac Colic, Jeffrey Hubbell and the other, anonymous, reviewer(s) for their contribution to the peer review of this work.

Reprints and permissions information is available at www.nature.com/reprints.

Publisher's note Springer Nature remains neutral with regard to jurisdictional claims in published maps and institutional affiliations.

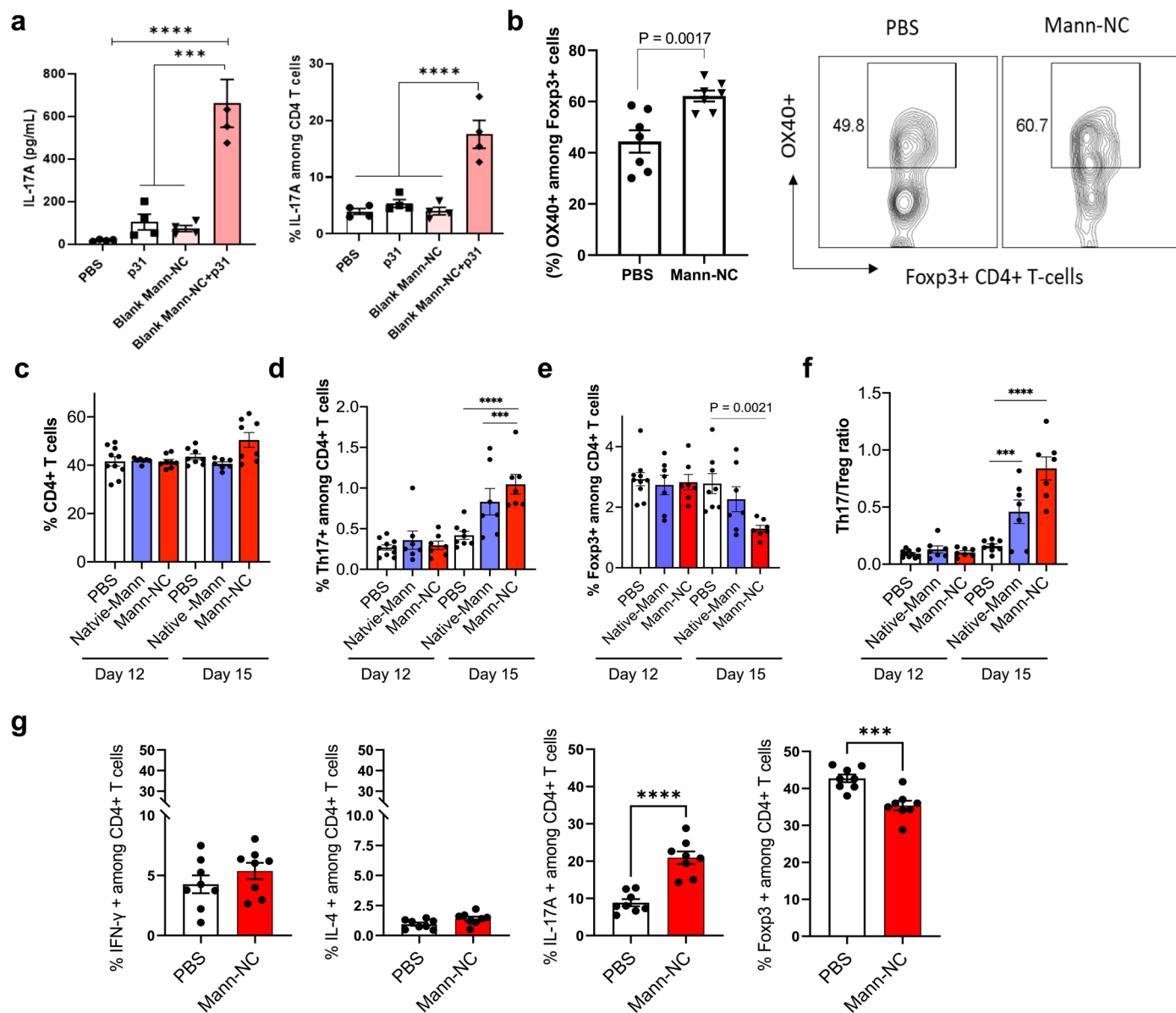
Springer Nature or its licensor (e.g. a society or other partner) holds exclusive rights to this article under a publishing agreement with the author(s) or other rightsholder(s); author self-archiving of the accepted manuscript version of this article is solely governed by the terms of such publishing agreement and applicable law.

© The Author(s), under exclusive licence to Springer Nature Limited 2022

**Extended Data Fig. 1 | A schematic illustration of Mann-NC synthesis.**

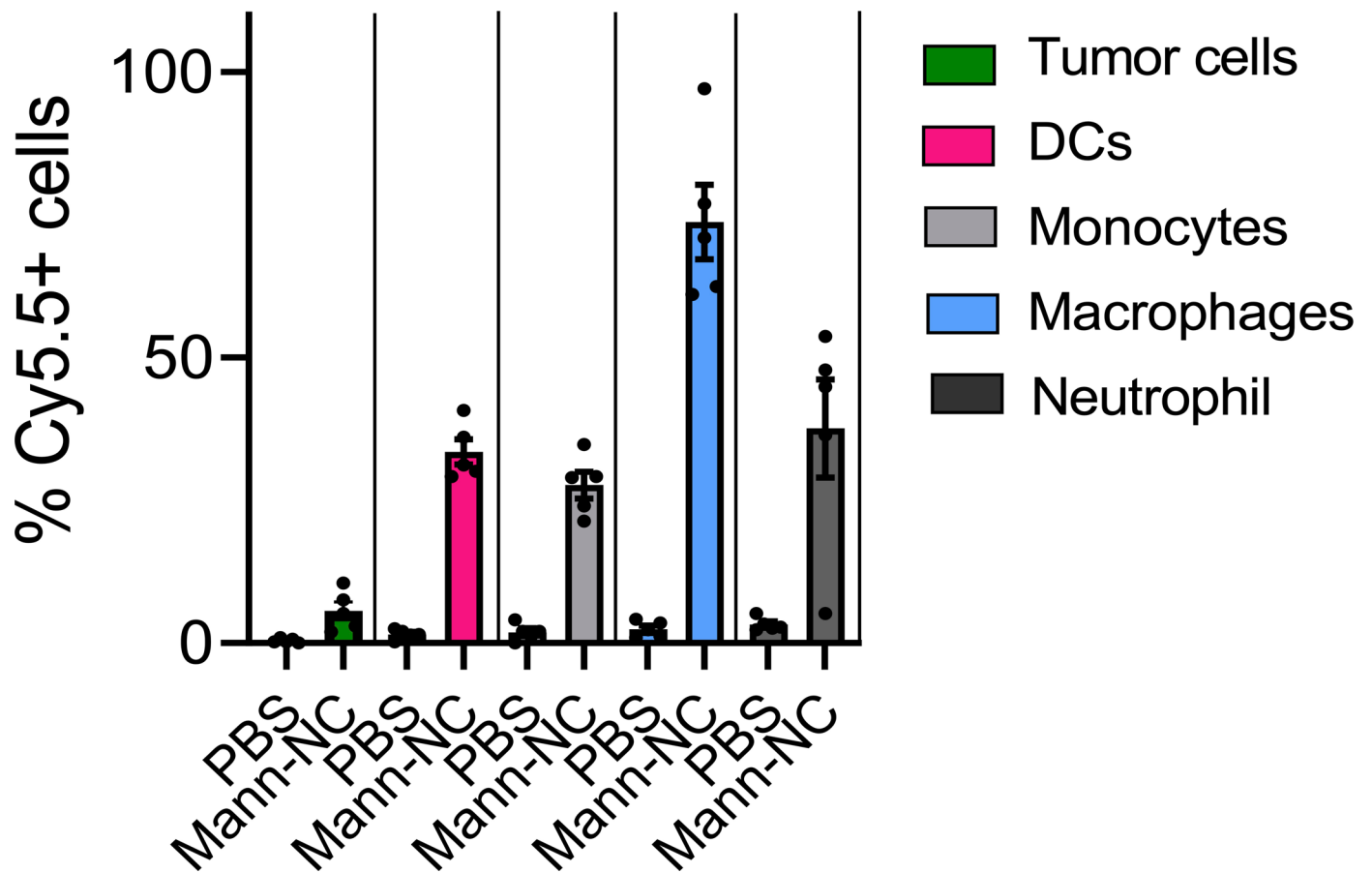
A negatively charged template silica nanoparticle was coated with branched polyethyleneimine (PEI, 25 kDa) polymer in ultra-pure water, followed by a chemical crosslinking step. The surface of PEI-coated silica nanoparticle was

reacted with oxidized mannan polymers by the aldehyde-amine reaction. Then the silica nanoparticle core was selectively removed, resulting in hollow Mann-NC entirely composed of mannan polymers.



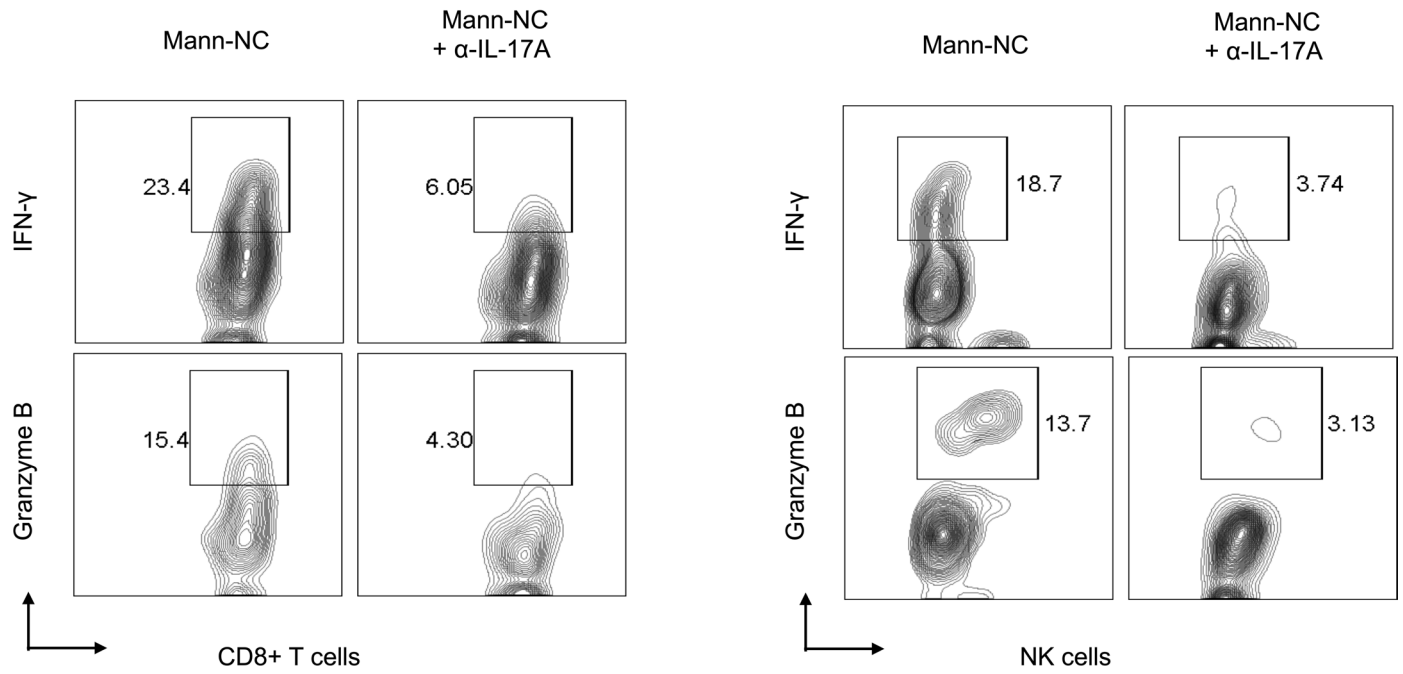
Extended Data Fig. 2 | Phenotype and activity of CD4 T cells induced by Mann-NC. (a) DCs stimulated by Mann-NC trigger the differentiation of CD4+ T-cells toward Th17 phenotype. BMDCs isolated from BDC2.5 TCR transgenic mice were treated with p31 MHC-II epitope with and without Mann-NC. After overnight incubation, p31-specific CD4+ T-cells from BDC2.5 TCR transgenic mice were added and cultured for 3 days. IL-17A released into the media was measured by ELISA, and CD4+ T-cells expressing IL-17A was measured by intracellular cytokine staining. (b) Mann-NC-inducing OX40 expression levels of Foxp3+ CD4+ T-cells and representative contour plots. (c-f) Tumor-draining lymph nodes were analysed for the frequencies of (c) CD4+ T-cells,

(d) IL17+ CD4+ Th17 cells, (e) Foxp3+ CD4+ Tregs, and (f) the corresponding Th17/Treg ratio. (g) CT26 tumor-bearing mice were treated with Mann-NC as in Fig. 3a, and CD4+ T-cells in the TME on day 15 were analysed for their subsets. Data represent mean \pm SEM, from a representative experiment (n = 4 (a); n = 7 (b); n = 7 for Native-Mann and Mann-NC, or 8 for PBS on day 15, or 10 for PBS on day 12 (c-f); or n = 8 (g) biologically independent samples) from two (a,b,g) or three (c-f) independent experiments. ***P < 0.001, ****P < 0.0001, analysed by one-way (a) or two-way (c-f) ANOVA with Bonferroni's multiple comparisons test or unpaired two-tailed Student's t-test (b,g).

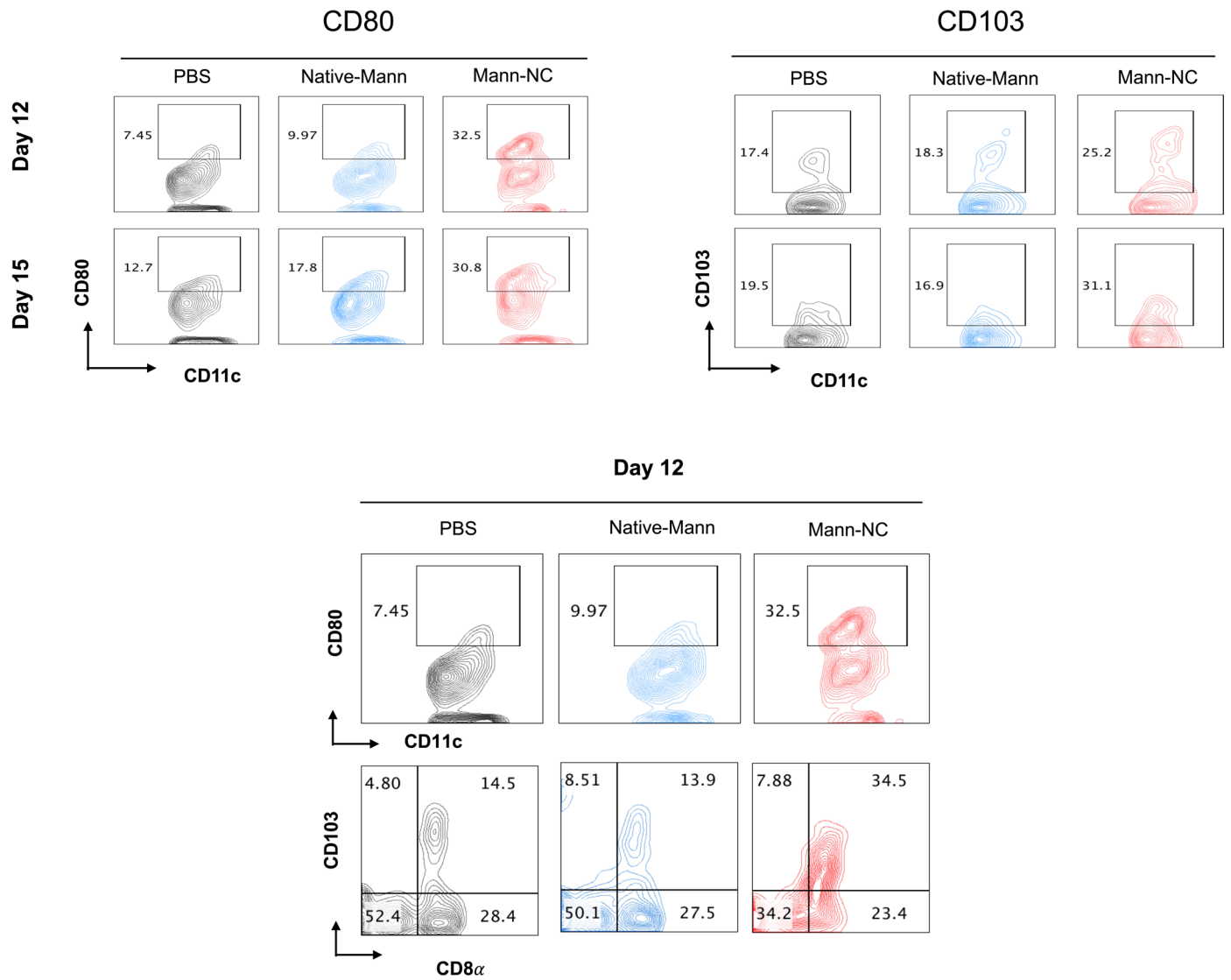


Extended Data Fig. 3 | Cellular uptake of Mann-NC among tumor cells and innate immune cells in local tumors. BALB/c mice were inoculated subcutaneously with 1.5×10^5 CT26 cells on day 0 and treated by intratumoral administration of Cy5.5-Mann-NC on day 9. After 3 days, tumor tissues were

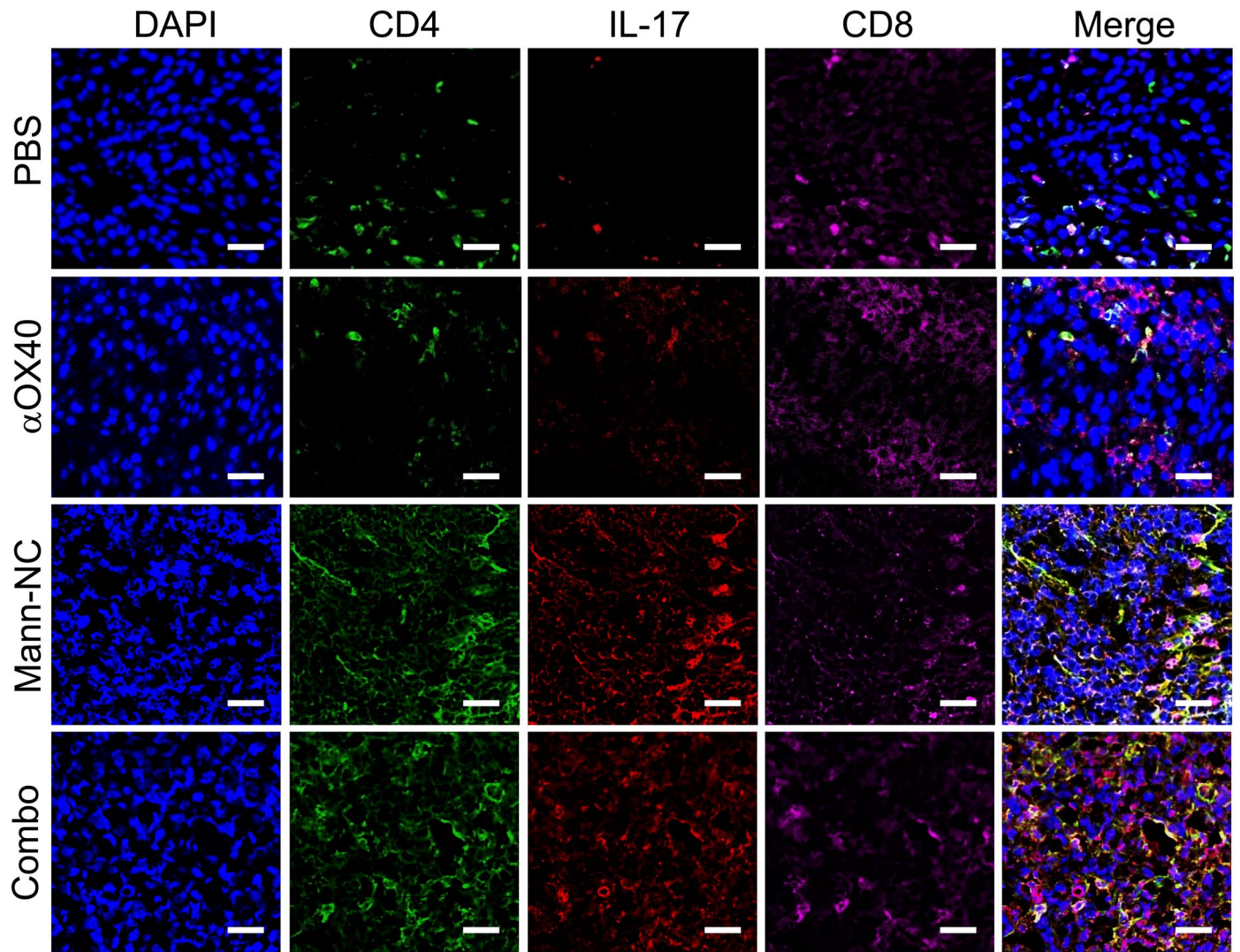
analysed for Cy5.5+ cells among CD45+ tumor cells, CD11c+ DCs, Ly6C+ monocytes, F4/80+ macrophages, and Ly6G+ neutrophils. Data represent mean \pm SEM, from a representative experiment with $n = 5$ biologically independent samples from two independent experiments.



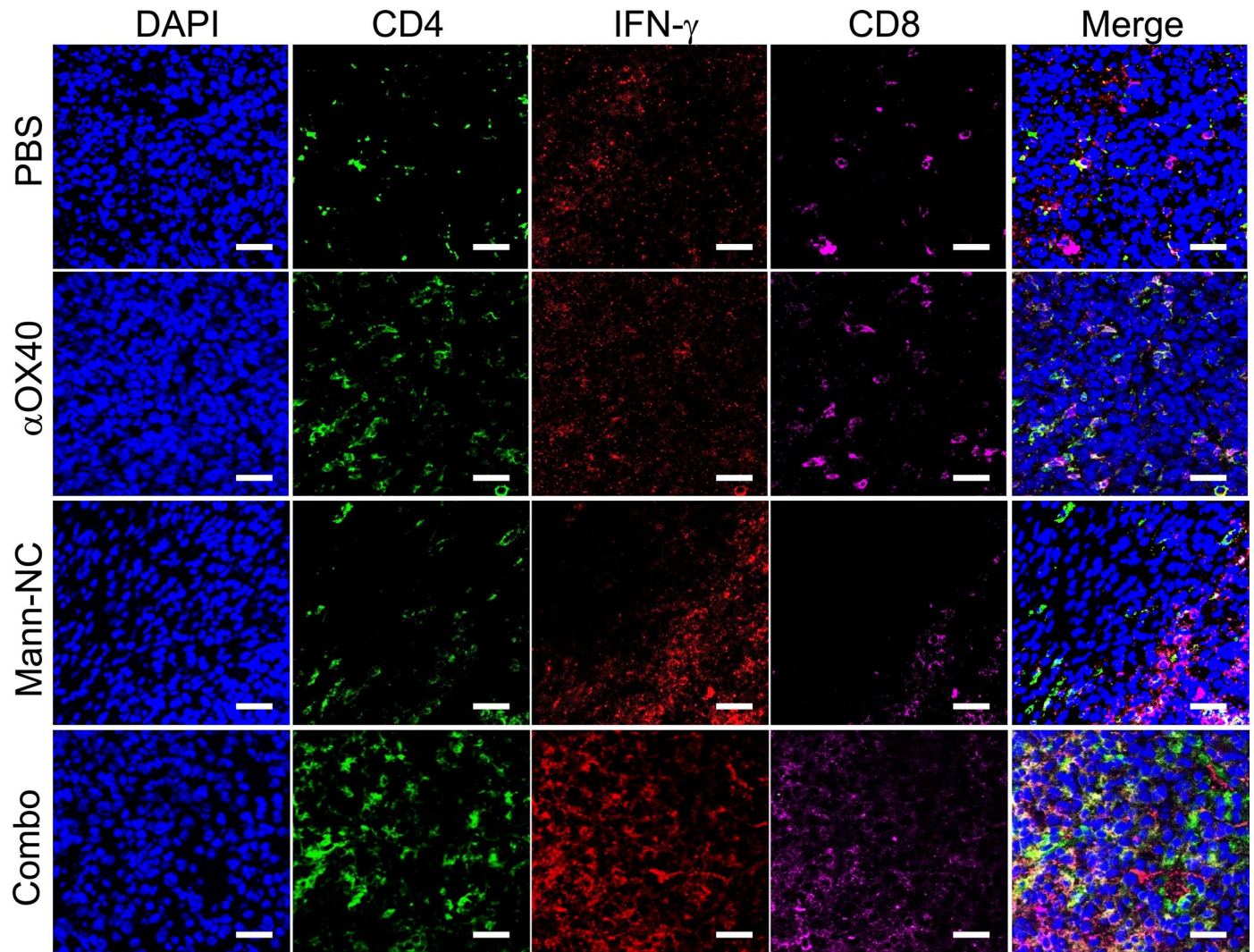
Extended Data Fig. 4 | Representative contour plots. Shown are representative contour plots of IFN- γ + CD8 T-cells, granzyme B + CD8 + T-cells, IFN- γ + NK cells, and granzyme B + NK cells for the dataset shown in the main Fig. 5e-f.



Extended Data Fig. 5 | Representative contour plots. Shown are the representative contour plots of CD80 + CD11c + DCs, CD103 + CD11c + DCs, and CD8 α + CD103 + CD11c + DCs for the dataset shown in the main Fig. 7a.



Extended Data Fig. 6 | Immunofluorescence analysis of IL-17A expression. Immunofluorescence images of IL-17A expression among CD4 T-cells and CD8 T-cells in TME on day 15. Scale bar represents 50 μ m.



Extended Data Fig. 7 | Immunofluorescence analysis of IFN- γ expression. Immunofluorescence images of IFN- γ expression among CD4 T-cells and CD8 T-cells in TME on day 15. Scale bar represents 50 μ m.

Reporting Summary

Nature Research wishes to improve the reproducibility of the work that we publish. This form provides structure for consistency and transparency in reporting. For further information on Nature Research policies, see our [Editorial Policies](#) and the [Editorial Policy Checklist](#).

Statistics

For all statistical analyses, confirm that the following items are present in the figure legend, table legend, main text, or Methods section.

n/a Confirmed

- | | | |
|-------------------------------------|-------------------------------------|--|
| <input type="checkbox"/> | <input checked="" type="checkbox"/> | The exact sample size (n) for each experimental group/condition, given as a discrete number and unit of measurement |
| <input type="checkbox"/> | <input checked="" type="checkbox"/> | A statement on whether measurements were taken from distinct samples or whether the same sample was measured repeatedly |
| <input type="checkbox"/> | <input checked="" type="checkbox"/> | The statistical test(s) used AND whether they are one- or two-sided
<i>Only common tests should be described solely by name; describe more complex techniques in the Methods section.</i> |
| <input type="checkbox"/> | <input checked="" type="checkbox"/> | A description of all covariates tested |
| <input type="checkbox"/> | <input checked="" type="checkbox"/> | A description of any assumptions or corrections, such as tests of normality and adjustment for multiple comparisons |
| <input type="checkbox"/> | <input checked="" type="checkbox"/> | A full description of the statistical parameters including central tendency (e.g. means) or other basic estimates (e.g. regression coefficient) AND variation (e.g. standard deviation) or associated estimates of uncertainty (e.g. confidence intervals) |
| <input type="checkbox"/> | <input checked="" type="checkbox"/> | For null hypothesis testing, the test statistic (e.g. F , t , r) with confidence intervals, effect sizes, degrees of freedom and P value noted
<i>Give P values as exact values whenever suitable.</i> |
| <input checked="" type="checkbox"/> | <input type="checkbox"/> | For Bayesian analysis, information on the choice of priors and Markov chain Monte Carlo settings |
| <input type="checkbox"/> | <input checked="" type="checkbox"/> | For hierarchical and complex designs, identification of the appropriate level for tests and full reporting of outcomes |
| <input checked="" type="checkbox"/> | <input type="checkbox"/> | Estimates of effect sizes (e.g. Cohen's d , Pearson's r), indicating how they were calculated |

Our web collection on [statistics for biologists](#) contains articles on many of the points above.

Software and code

Policy information about [availability of computer code](#)

Data collection Flow cytometric data were collected using a Ze5 cell analyzer (BD Biosciences). In vitro cell images were acquired using a Leica SP8 confocal microscope. DLS analysis was collected in Zetasizer software version 7.13. Transmission electron microscope (TEM) images were acquired using JEOL 1400-plus, and atomic force microscope (AFM) was performed using Asylum-1 MFP-3D.

Data analysis Flow-cytometry analysis was done in FlowJo (v.10.2) (Tree Star). In vitro cell images were analysed using Image J Software(V 1.8.0). Statistical analysis was done in GraphPad Prism 6.0. DLS analysis was done in Zetasizer software version 7.13.

For manuscripts utilizing custom algorithms or software that are central to the research but not yet described in published literature, software must be made available to editors and reviewers. We strongly encourage code deposition in a community repository (e.g. GitHub). See the Nature Research [guidelines for submitting code & software](#) for further information.

Data

Policy information about [availability of data](#)

All manuscripts must include a [data availability statement](#). This statement should provide the following information, where applicable:

- Accession codes, unique identifiers, or web links for publicly available datasets
- A list of figures that have associated raw data
- A description of any restrictions on data availability

The main data supporting the results in this study are available within the paper and its Supplementary Information. Source data for tumour size are provided with this paper. All data generated in this study are available from the corresponding authors on reasonable request.

Field-specific reporting

Please select the one below that is the best fit for your research. If you are not sure, read the appropriate sections before making your selection.

Life sciences Behavioural & social sciences Ecological, evolutionary & environmental sciences

For a reference copy of the document with all sections, see [nature.com/documents/nr-reporting-summary-flat.pdf](https://www.nature.com/documents/nr-reporting-summary-flat.pdf)

Life sciences study design

All studies must disclose on these points even when the disclosure is negative.

Sample size	Sample sizes were chosen on the basis of preliminary data from at least two pilot experiments and of previously published results in the literature.
Data exclusions	No data were excluded.
Replication	All experiments were repeated at least twice, with similar results.
Randomization	Mice were assigned randomly to the experimental groups.
Blinding	The investigators were not blinded to group allocation during the experiments and outcome assessments because the data analyses were based on objectively measurable data.

Reporting for specific materials, systems and methods

We require information from authors about some types of materials, experimental systems and methods used in many studies. Here, indicate whether each material, system or method listed is relevant to your study. If you are not sure if a list item applies to your research, read the appropriate section before selecting a response.

Materials & experimental systems

n/a	Involved in the study
<input type="checkbox"/>	<input checked="" type="checkbox"/> Antibodies
<input type="checkbox"/>	<input checked="" type="checkbox"/> Eukaryotic cell lines
<input checked="" type="checkbox"/>	<input type="checkbox"/> Palaeontology and archaeology
<input type="checkbox"/>	<input checked="" type="checkbox"/> Animals and other organisms
<input checked="" type="checkbox"/>	<input type="checkbox"/> Human research participants
<input checked="" type="checkbox"/>	<input type="checkbox"/> Clinical data
<input checked="" type="checkbox"/>	<input type="checkbox"/> Dual use research of concern

Methods

n/a	Involved in the study
<input checked="" type="checkbox"/>	<input type="checkbox"/> ChIP-seq
<input type="checkbox"/>	<input checked="" type="checkbox"/> Flow cytometry
<input checked="" type="checkbox"/>	<input type="checkbox"/> MRI-based neuroimaging

Antibodies

Antibodies used

Anti-CD16/CD32 (93, 14016186, eBioscience), Anti-mouse CD11c-FITC (N418, 11-0114-81, eBioscience), anti-CD86 rat monoclonal antibody-FITC (GL-1, 105006, BioLegend), anti-CD3 (145-2C11, 100301, Biolegend), anti-CD28 (37.51, 102101, Biolegend), CD4 monoclonal antibody-PE (GK1.5, 12-0041-82, eBioscience), anti-mouse IFN- γ -PE (XMG1.2, 505825, Biolegend), CD25 Rat anti-mouse-BV605 (PC61, 563061, BD Biosciences), IL-4 Rat anti-Mouse-BV 605 (11B11, 564007, BD Biosciences), Foxp3 Rat anti-mouse-PE (MF23, 560408, BD Biosciences), IL-17A Rat anti-mouse-FITC (eBio17B7, 11-7177-81, eBioscience), CD8 α (2.43, BP0061, Bio X cell), CD4 (GK1.5, BP0003-1, Bio X cell), Anti Asialo GM1 (Rabbit, 986-10001, Wako chemicals USA), Ly6G (1A8, BP0075-1, Bio X cell), Isotype control Immunoglobulin G 2b (LTF-2, BP0090, Bio X cell), CD45-FITC (30-F11, 11-0451-81, eBioscience), CD8 α -APC (53-6.7, 553035, BD Biosciences), CD3 Molecular Complex Rat anti-Mouse-PE-Cy7(17A2, 560591, BD Biosciences), CD4 Rat anti-Mouse-APC (GK1.5, 12-0041-82, eBioscience) CD86 Rat anti Mouse-PE-Cy7 (GL1, 560582, BD Biosciences), NK1.1 anti-Mouse-PE (12-5941-82, eBioscience), Anti-mouse F4/80 (PE, BM8, 123109, BioLegend), anti-mouse CD206 (APC, C068C2, 141708, BioLegend), anti-Ly6C-FITC (AL-21, 553104, BD Biosciences), and CD134 (OX40, OX-86, 14-1341-82, eBioscience), IL-17A (17F3, BP0173, Bio X cell), Dectin-2 (D2.11E4, MCA2415T, Bio-Rad), TLR4-MD-2 complex (MTS510, 14-9924-82, eBioscience), TLR2 (CD282, 6C2, 14-9021-80, eBioscience), Dectin-1 (2A11, MCA2289T, Bio-Rad), F4/80-APC/Cy7 (BM8, 123118, BioLegend), CD86-FITC (GL-1, 105006, BioLegend), CD103-FITC (2E7, 121419, BioLegend), Ly-6G-PE (1A8, 127607, BioLegend), CD11b-APC/Cy7 (M1/70, 557657, BD Biosciences), CD11b-Brilliant Violet 605 (M1/70, 101237, BioLegend), Granzyme B-FITC (QA16A02, 372206, BioLegend), I-A/I-E-PerCP/Cyanine5.5 (M5/114.15.2, 107625, BioLegend), CD49b-PerCP/Cyanine5.5 (M α 2, 103519, BioLegend), Dectin-2/CLEC6A alpha – APC (Polyclonal, FAB1525A, R&D system), CD3 (17A2, MAB4841-100, R&D system), IFN- γ (Polyclonal, AF-585-NA, R&D system), IL-17A (Polyclonal, AF-421-NA, R&D system), Integrin alpha 2/CD49b (Polyclonal, AF1740, R&D system), CD4 (Polyclonal, NBP1-19371, Novus Biologicals), CD8 (53-6.7, NBP1-49045, Novus Biologicals), Goat anti-rabbit IgG H&L - Alexa Flour 488 (Polyclonal, ab150077, Abcam), Donkey anti-sheep IgG H&L - Alexa Flour 488 (Polyclonal, ab150177, Abcam), Donkey anti-goat IgG H&L - Cy3 (Polyclonal, Abcam, #ab6949), Goat anti-rat IgG H&L - Alexa Flour 647 (Polyclonal, A-21247, Invitrogen).

Validation

Antibody validation was provided by manufacture's website (cell images) and/or data is provided in the paper.

Eukaryotic cell lines

Policy information about [cell lines](#)

Cell line source(s)	CT26, MC38 and B16F10 cell lines were obtained from the American Type Culture Collection (ATCC). NOOC1 single-cell clones were isolated from the visible oral squamous cell carcinoma lesions of C57BL/6J mice treated with 4NQO-containing drinking water for 16 weeks.
Authentication	Cells were used as received from ATCC without further authentication.
Mycoplasma contamination	All cell lines tested negative for mycoplasma contamination.
Commonly misidentified lines (See ICLAC register)	No commonly misidentified cell lines were used.

Animals and other organisms

Policy information about [studies involving animals](#); [ARRIVE guidelines](#) recommended for reporting animal research

Laboratory animals	For the in vivo studies, 6–8 weeks-old female BALB/c mice (Jackson Laboratory, 18–20 g) and C57BL/6 mice (Jackson Laboratory, 18–20 g) were used. NOD.BDC2.5 transgenic mice (5–7 weeks gold female or male, 15–20 g) were obtained from the Jackson Laboratory. Mice were housed in 12-hour light–dark cycle, at 72 F, and about 30% humidity.
Wild animals	The study did not involve wild animals.
Field-collected samples	The study did not involve samples collected from the field.
Ethics oversight	All work performed on animals was in accordance with, and approved by, the Institutional Animal Care & Use Committee (IACUC) at University of Michigan, Ann Arbor.

Note that full information on the approval of the study protocol must also be provided in the manuscript.

Flow Cytometry

Plots

Confirm that:

- The axis labels state the marker and fluorochrome used (e.g. CD4-FITC).
- The axis scales are clearly visible. Include numbers along axes only for bottom left plot of group (a 'group' is an analysis of identical markers).
- All plots are contour plots with outliers or pseudocolor plots.
- A numerical value for number of cells or percentage (with statistics) is provided.

Methodology

Sample preparation	Sample preparation is described in Methods.
Instrument	Ze5 cell analyzer (BD Biosciences).
Software	Ze5 cell analyzer (BD Biosciences) was used for data collection. FlowJo were used for data analysis.
Cell population abundance	Data on the abundance of relevant cell populations are provided in the paper.
Gating strategy	Cells were gated first by morphology to exclude cell debris, doublets were then gated out by SSC-A/SSC-W, followed by exclusion of dead cells by gating on dye-negative cells.

Tick this box to confirm that a figure exemplifying the gating strategy is provided in the Supplementary Information.